CANCER

Serial multiomics uncovers anti-glioblastoma responses not evident by routine clinical analyses

Alexander L. Ling[1]†, Jennifer Gantchev[2]†, Michael C. Prabhu[3,4]†, Sreyashi Basu[5]†, Ryuhjin Ahn[6]†, Alicia D'Souza[6]†, Nafisa Masud[1], Anna Ball[1], Odysseas Nikas[1], Genaro R. Villa[1], Michael S. Regan[2], Gerard Baquer[2], Georges Ayoub[3,4], Charles A. Whittaker[6], Zaki Abou-Mrad[7], Andres Santos[1,3], Charles P. Couturier[2,6,8,9], Dina Elharouni[3,4], Jayne Vogelzang[3,4], Kenny K. H. Yu[7], Hong Chen[5], Zhong He[5], Wen Jiang[10], Calixto Hope Lucas[11], Haley E. Sax[12], Frederick F. Lang[13], Vinay K. Puduvalli[14], Viviane Tabar[7], Cameron W. Brennan[7], Adrienne Boire[15], Matthias Holdhoff[16], Chetan Bettegowda[17], Michael Cima[6], Isaac H. Solomon[3,4], Ying Yuan[18], Paul P. Tak[19], Accelerating GBM Therapies TeamLab[20]‡, Padmanee Sharma[5,21]*, Forest M. White[6]*, Keith L. Ligon[3,4]*, Nathalie Y.R. Agar[2]*, David A. Reardon[22]*, Giacomo Oliveira[8,12]*, E. Antonio Chiocca[1]*

Recurrent glioblastoma (rGBM) remains incurable. One barrier to the development of effective rGBM therapies is the difficulty in collecting posttreatment tumor tissue. Serial multiomic assays from longitudinal rGBM biopsies may uncover tumor responses to a treatment. Here, we obtained 97 serial rGBM biopsy cores over 4 months from the first two patients participating in a clinical trial of repeated intratumoral dosing of the immunotherapeutic agent CAN-3110. Multiomic analysis of the biopsy cores revealed therapeutic effects, including longitudinal and spatial reshaping of the rGBM's microenvironment, expansion of new T cell tissue-resident effector memory clonotypes against CAN-3110 epitopes and other undetermined antigens, and expression of human leukocyte antigen (HLA)–presented immunopeptides, including cancer testis antigens. Moreover, serial integrated multimodal analyses provided evidence of therapeutic responses to CAN-3110 despite traditional magnetic resonance imaging indicating progression. Clinically, the two treated patients achieved a pathologic response or stable clinical disease, respectively. These results show the value of longitudinal tissue sampling to understand rGBM's evolution during administration of an investigational therapy.

INTRODUCTION

Effective therapies for glioblastoma (GBM) remain elusive, with most patients dying within 2 years of diagnosis (*1*, *2*). Evidence demonstrating biological effects of new therapeutics is critical to support advancement to later-stage trials. Current evaluation of treatment outcome relies on changes in gadolinium enhancement or T2/FLAIR (fluid-attenuated inversion recovery) hyperintensity of brain magnetic resonance imaging (MRI). However, these surrogate assessments cannot determine whether the trial's therapeutic agent successfully engaged its hypothesized target, nor can they determine whether progressive MRI findings are because of accumulating underlying tumor or inflammatory changes associated with prior treatment, such as radiation therapy. For some therapeutics, such as immunotherapies, MRI changes can mimic tumor recurrence, making it difficult to know whether the intervention was successful. Thus, reliance on MRI changes to accurately assess response among patients with GBM is often limited and can be misleading.

Recognizing these limitations, window-of-opportunity trials and phase 0 trials have been used in the clinical development of some therapies for GBM (*3*–*5*). In both approaches, a posttreatment tumor specimen, typically obtained after a short exposure to an investigational therapy, can be used to determine the extent to which a therapy crosses the blood-brain barrier, engages its molecular target, or alters the tumor microenvironment (TME) (*6*–*8*). Given that these approaches

[1]Harvey Cushing Neuro-Oncology Laboratories, Department of Neurosurgery and Center for Tumors of the Nervous System, Mass General Brigham Cancer Institute and Harvard Medical School, Boston, MA 02115, USA. [2]Surgical Brain Mapping and Molecular Imaging Laboratory, Department of Neurosurgery, Mass General Brigham Cancer Institute and Harvard Medical School, Boston, MA 02115, USA. [3]Department of Pathology, Mass General Brigham Cancer Institute and Harvard Medical School, Boston, MA 02115, USA. [4]Department of Pathology, Dana-Farber Cancer Institute and Harvard Medical School, Boston, MA 02115, USA. [5]James P. Allison Institute, University of Texas MD Anderson Cancer Hospital, Houston, TX 77030, USA. [6]Koch Institute for Integrative Cancer Research, Massachusetts Institute of Technology, Cambridge, MA 02139, USA. [7]Department of Neurosurgery, Memorial Sloan Kettering Cancer Center, New York, NY 10065, USA. [8]Broad Institute, Massachusetts Institute of Technology, Cambridge, MA 02139, USA. [9]Department of Neurology and Neurosurgery, McGill University, Montreal, QC H3AOG4, Canada. [10]Department of Radiation Oncology, University of Texas MD Anderson Cancer Hospital, Houston, TX 77030, USA. [11]Department of Pathology, Johns Hopkins University Medical Center, Baltimore, MD 21205, USA. [12]Department of Medical Oncology, Dana-Farber Cancer Institute and Harvard Medical School, Boston, MA 02115, USA. [13]Department of Neurosurgery, University of Texas MD Anderson Cancer Hospital, Houston, TX 77030, USA. [14]Department of Neuro-Oncology, University of Texas MD Anderson Cancer Hospital, Houston, TX 77030, USA. [15]Department of Neurology, Human Oncology and Pathogenesis Program, Memorial Sloan Kettering Cancer Center, New York, NY 10065, USA. [16]Division of Neuro-Oncology, Sidney Kimmel Comprehensive Cancer Center, Johns Hopkins University Medical Center, Baltimore, MD 21205, USA. [17]Department of Neurosurgery, Johns Hopkins University Medical Center, Baltimore, MD 21205, USA. [18]Department of Biostatistics, University of Texas MD Anderson Cancer Hospital, Houston, TX 77030, USA. [19]Candel Therapeutics Inc., Needham, MA 02494, USA. [20]Accelerating GBM Therapies TeamLab, Cambridge, MA 02142, USA. [21]Department of Immunology, University of Texas MD Anderson Cancer Hospital, Houston, TX 77030, USA. [22]Center for Neuro-Oncology, Dana-Farber Cancer Institute and Harvard Medical School, Boston, MA 02115, USA.
*Corresponding author. Email: padsharma@mdanderson.org (P.S.); fwhite@mit.edu (F.M.W.); keith_ligon@dfci.harvard.edu (K.L.L.); nagar@bwh.harvard.edu (N.Y.R.A.); david_reardon@dfci.harvard.edu (D.A.R.); giacomo_oliveira@dfci.harvard.edu (G.O.); eachiocca@mgb.org (E.A.C.)
†These authors contributed equally to this work.
‡Accelerating GBM Therapies TeamLab members and affiliations are listed at the end of this paper.

assess only a single point in time, they do not provide important information about the complex evolutionary changes in the biology of GBMs over the course of multiple treatments as a function of the investigational agent. Moreover, a single time point of sampling may not correspond with the time of optimal biological activity of the investigational agent and may miss important biological events in response to treatment. Approaches that include longitudinal sampling of the tumor before and at multiple predefined time points after therapy administration could address this shortcoming (*9*–*12*).

There has been reluctance to institute a longitudinal GBM biopsy paradigm in clinical trials because of concerns related to safety, costs, sampling bias, ethical issues, and patient exposure to multiple surgeries. Liquid biopsies have been advocated as alternatives to surgical biopsy for longitudinal analyses, but to date, these have been limited to genomic or proteomic assays and have not provided a complete representation of the complex changes occurring in GBM tumors and the cellular microenvironment (*13*, *14*). There is an unexplored opportunity to safely study the therapeutic perturbations imposed on GBM tumors during a trial on the basis of the recent confluence of sophisticated molecular pathology technologies using small tissue samples (*15*); exquisite bioinformatics for analyses of cellular, molecular, and immunologic phenotypes and genotypes at the DNA, RNA, protein, and metabolite level (referred to as multiomics) (*15*); and increased precision and safety of modern neurosurgical image-guided biopsy techniques.

We initiated a feasibility study of serial planned tumor biopsies (pretreatment baseline plus up to five time points over 4 months) in patients with recurrent GBM (rGBM) with concomitant intratumoral injection of the oncolytic herpes simplex virus 1 (HSV1) CAN-3110 (*16*) at each time point. Ninety-seven serial multisector biopsies were collected for the first two patients in this trial and were analyzed by spatial tumor cyclic immunofluorescence (CyCIF), single-cell RNA sequencing (scRNA-seq), proteomics, phosphoproteomics, immunopeptidomics, and tumor T cell clonotype characterization, in addition to traditional histopathologic techniques, to longitudinally map the cellular and molecular evolution of the rGBM to immunotherapeutic perturbation by CAN-3110 (clinicaltrials.gov: NCT03152318). Serial analyses from these two patients support that serial CAN-3110 administration reshapes the TME both spatially and longitudinally, with influx of immune cells expressing markers and transcripts consistent with antitumor activity. Of relevance, tumor expansion of T cell clonotypes temporally matched up-regulation of human leukocyte antigen (HLA) expression and expression of several immunopeptidomes, some of which have been reported to be cancer and testis antigens; we also identified the expansion of T cell clones against CAN-3110 epitopes. Although traditional MRI analyses for both patients showed changes consistent with tumor progression by standard radiologic assessment in neuro-oncology (RANO) criteria (*17*–*19*), the multiomic analyses coupled with histopathologic and clinical outcomes revealed evidence of positive pharmacodynamic and therapeutic effects. Therefore, our report supports the potential value of longitudinal analyses of rGBM samples acquired at predefined time points during a clinical trial of investigational therapy.

RESULTS

Trial timeline and rGBM biopsy allocation

Per protocol, the longitudinal biopsies and intratumoral doses of CAN-3110 were designed to be carried out over 120 days (Fig. 1A). Among the first two patients enrolled in this trial, expected to accrue a total of 12 participants, a total of 80 rGBM biopsies were harvested before each CAN-3110 intratumoral injection over 4 months, including 6 to 13 biopsies per time point per patient, with an additional 17 biopsies collected in a posttrial resection for DFCI1 (one of the two patients in the trial). Each biopsy was obtained stereotactically at a location different from the planned CAN-3110 injection site. At the time of repeat treatment, biopsies were obtained from the approximate site of the prior injection. Tumor material was processed as fresh, snap-frozen, or paraffin-embedded samples on the basis of a tumor tissue prioritization algorithm and allocated for multiomic analyses, including traditional histopathology, bulk and scRNA-seq, multiplex immunofluorescence, proteomics/phosphoproteomics and immunopeptidomics (Fig. 1B). Tumor, cerebrospinal fluid (CSF), and peripheral blood mononuclear cell (PBMC) samples were also banked for possible additional future analyses. This finding demonstrated that the planned longitudinal procurement of GBMs could be performed successfully.

Clinicopathologic and imaging outcomes

Both patients (DFCI1 and DFCI2) tolerated the serial tumor biopsy and CAN-3110 injection procedures well without dose-limiting toxicities (tables S1 and S2). Data file S1 illustrates the time course of MRI scans with the concomitant routine histopathologic exam of each serially collected biopsy core collected right before each CAN-3110 dose for each patient. Traditional histopathologic examination of day 0 biopsy cores revealed infiltrating glioma mixed with some treatment effect (necrosis and gliosis). Progressively increased contrast enhancement consistent with recurrent tumor was observed on serial MRI scans obtained during study therapy before each treatment for both patients (Fig. 2A, fig. S1A, and data file S1). In contrast, serial biopsies after initiation of study therapy showed an increased proportion of reactive cells, plasma cells, lymphocytes, and mononuclear cells, consistent with an immune reactive process, and decreased microscopic tumor content relative to the pretreatment baseline for both patients, with no evidence supporting a demyelinating process (data file S1).

Patient DFCI1, a 56-year-old, right-handed male, developed progression of a right frontal GBM (*IDH*, isocitrate dehydrogenase, wild type; *MGMT*, O6-methylguanine-DNA methyltransferase, partially methylated) 50 weeks after initial diagnosis that was followed by standard chemoradiation and four cycles of adjuvant temozolomide. The study therapy was initiated 5 months after completion of radiation therapy. While on the study therapy, 26 biopsy cores were collected from six biopsy locations along four needle tracks across four successive CAN-3110 injection time points over 63 days. An additional 17 tumor biopsies were collected from three locations during a posttrial resection 106 days after the first CAN-3110 injection. MRI scans after each biopsy/injection were annotated with the anatomic regions of the biopsy(ies)/injection(s) (fig. S1A, data file S1, and movie S1). Traditional MRI after 3 months on the study therapy suggested continued tumor growth and led the patient and physicians to stop the trial; the patient underwent a craniotomy to resect the mass 106 days after initiation of the study therapy. Histopathologic findings revealed substantial inflammatory infiltrates, necrosis with treatment effect, and infrequent microscopic tumor cells (data file S1). The patient then was treated with an immune checkpoint inhibitor, but a subsequent MRI was interpreted as progression (fig. S1A and data file S1). At this point, the patient decided to

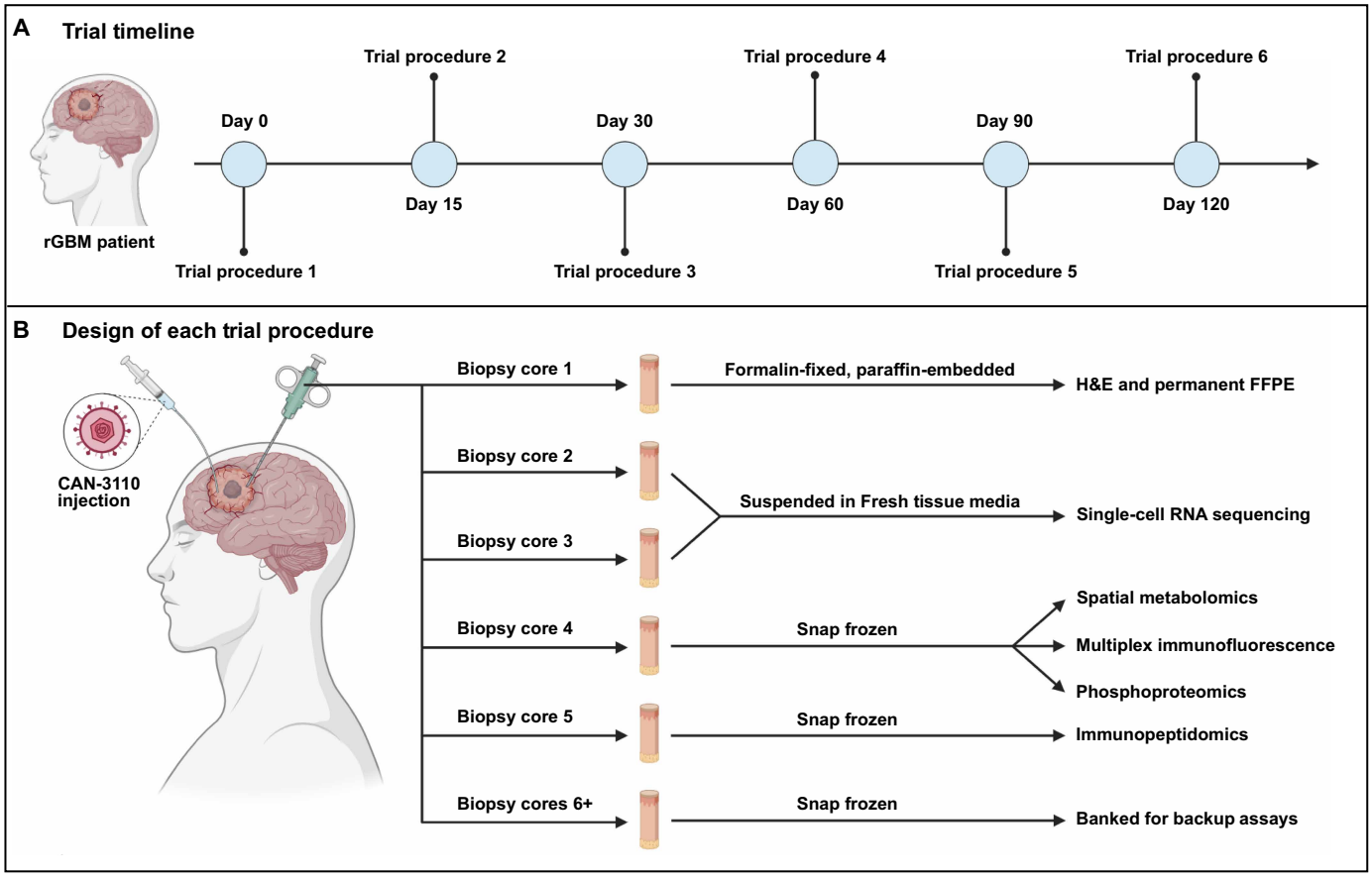

Fig. 1. Clinical trial schema and tissue allocation. (**A**) Schematic timeline of serial GBM stereotactic biopsy and longitudinal stereotactic intratumoral injections of CAN-3110 oncolytic HSV1 (formerly known as rQNestin34.5v.2) (*61*) on approximately days 0, 15, 30, 60, 90, and 120. The protocol timing allowed a few days difference from these times, explaining why, in subsequent figures, labels, and text indicate days that are slightly different (e.g., day 16 instead of day 15 or day 119 instead of day 120). (**B**) Design showing use of serial locoregional investigative biopsies obtained before successive injections of CAN-3110. Stereotactic biopsies were preplanned for pathology, spatial imaging, and multiomic analyses. FFPE, formalin-fixed, paraffin-embedded.

discontinue further therapy and to focus on quality of life. He remained active with his family and continued his work for ~3 months. He decided to pursue comfort measures only in an inpatient hospice facility, where he died ~12 months from initiation of the study therapy and 20 months from original GBM diagnosis. Brain autopsy revealed further mixed findings, including a necrotic tumor mass with inflammatory cells and some infrequent tumor cell infiltration in the right cortex and into the corpus callosum with no demyelination or evidence of brain inflammatory changes (fig. S1B). There was no tumor in the brainstem. The cause of death was indeterminate because only a brain postmortem had been consented to.

Patient DFCI2, a 66-year-old, right-handed woman initially underwent resection of a left parieto-occipital GBM (*IDH* wild type; MGMT unmethylated), followed by standard radiochemotherapy and six cycles of adjuvant temozolomide. She developed local tumor progression after ~21 months of surveillance follow-up and enrolled in this trial. Figure 2A, fig. S1A, data file S1, and movie S2 illustrate the time course of MRI scans with the concomitant routine histopathologic exam of each serial biopsy collected right before each CAN-3110 dose. She underwent the planned six stereotactic tumor biopsy procedures with intratumoral CAN-3110 administration over 120 days, yielding 54 tumor biopsy cores from 12 biopsy locations along nine needle tracks. After her initial CAN-3110 dose, subsequent tumor biopsies throughout the study revealed ongoing inflammatory changes and minimal residual tumor. She remained clinically stable for 18 months, although serial MRI scans revealed continued local enhancement (fig. S1A and data file S1). At 18 months, a brain MRI revealed evidence of new enhancement along the splenium as she developed a right hemiparesis and dysphasia (data file S1). Salvage systemic therapy with bevacizumab and niraparib was initiated, and the patient remains alive.

Longitudinal spatial evolution was observed in CAN-3110–treated rGBMs

MRI follow-up showed no radiographic response to treatment in either patient, with rapid growth of enhancing lesions in both patients continuing posttreatment (Fig. 2A). However, the longitudinal collection of tissues in these patients allowed us to assess molecular and cellular changes in these tumors over time that were not apparent through radiographic imaging. Tumor content at each biopsy location was assessed by digital pathology assessment (fig. S2) and CyCIF (fig. S3) (*20*, *21*). Pathological assessment by

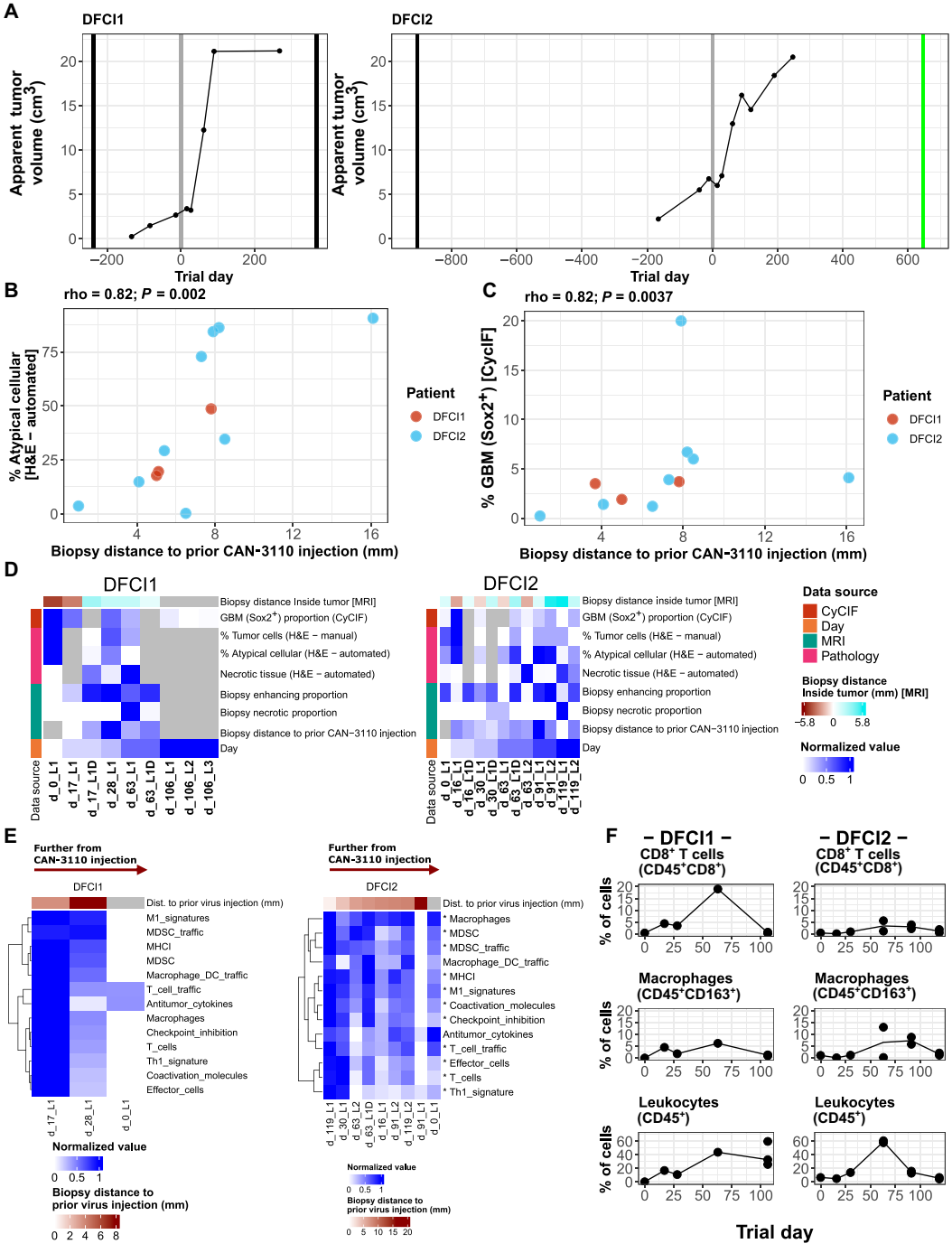

Fig. 2. Proximity to CAN-3110 injection is associated with decreased tumor content and increased immune signature scores. (**A**) Enhancing tumor volumes as assessed by MRI across time. The vertical black bar on the left indicates initial GBM diagnosis; day 0 = day of first CAN-3110 injection; vertical right bar indicates last follow-up (black = deceased, green = alive). (**B**) Pathological assessment of the percentages of each slide containing atypical cellular regions using automated digital H&E quantification versus the distance biopsies were taken from nearest prior CAN-3110 injection site. Spearman's rank correlation rho and *P* value are shown above the plot. Also see fig. S2. (**C**) GBM ($Sox2^+$) cell frequencies as measured by CyCIF versus the distance biopsies were taken from nearest prior CAN-3110 injection site. Spearman's rank correlation rho and *P* value are shown above the plot. Also see fig. S3. (**D**) Heatmaps ordered by time showing GBM cell frequency (as determined by CyCIF $Sox2^+$), pathological quantifications, and MRI metrics for each biopsy site. Gray cells indicate missing data. The day 106 samples from DFCI1 are from an off-trial resection in which precise tissue collection locations could not be determined. This prevented calculation of MRI metrics for these locations. (**E**) Heatmaps of bulk RNA-seq ssGSEA signatures that were previously shown to be correlated with CAN-3110 patient response (*16*) with biopsy sites ordered by distance from nearest prior CAN-3110 virus injection site. The plotted normalized score values were calculated by taking robust *z*-score–normalized ssGSEA scores and scaling these *z* scores between 0 and 1 for each signature. An * indicates signatures that are correlated with distance to prior injection site (FDR < 0.2) using Pearson correlation testing (two-sided based on *t* distribution). (**F**) Immune cell quantifications from CyCIF over time in DFCI1 (top) and DFCI2 (bottom). Also see fig. S3.

hematoxylin and eosin (H&E) staining revealed wide variations in atypical cellular regions and tumor cell percentages by collection site and time point (figs. S2 and S4, A and B), with CyCIF staining of Sox2 showing tumor cell proportions of <5% in most sampling locations, with a steady decrease in GBM cell proportion over time for DFCI1 (figs. S3 and S4C). Although Sox2 staining was nominally correlated with H&E-based measures of atypical cellular regions, $Sox2^+$ proportions varied from 4 to 20% in samples assessed as >80% atypical cellular regions by H&E (fig. S4D), suggesting substantial cellular locoregional heterogeneity not readily apparent by routine pathology.

Both atypical cellular regions (as determined by automated H&E quantification) and tumor cell proportions (as determined by $Sox2^+$ CyCIF) were significantly correlated ($P = 0.0020$ and $P = 0.0037$, respectively) with distance from the nearest prior CAN-3110 tumor administration site, with higher tumor proportions associated with farther distance from treatment (Fig. 2, B and C). However, the manual pathologist quantification of tumor cell percentages from H&E slides did not show a significant reduction (fig. S4, E and F). Conversely, CyCIF and pathological assessments of tumor content were not associated with MRI enhancement (Fig. 2D) or spatial location (fig. S4G).

Tumor cells were further assessed by scRNA-seq using copy number variation (CNV) inference to identify neoplastic cells (fig. S5, A and B), followed by classification into tumor cell transcriptional subtypes (*22*). DFCI2's samples contained too few neoplastic cells to assess. The analysis of samples from DFCI1 showed a shift from astrocyte (AC)–like to mesenchymal (MES)–like neoplastic cells after CAN-3110 treatment (fig. S5, C to E).

Given the observed relationship between tumor content and CAN-3110 tumor injection site, we hypothesized that immune activation may also be spatially related to CAN-3110 location. To test this, we applied single-sample gene set enrichment analysis (ssGSEA) on bulk RNA-seq data from the collected biopsies to assess 13 immune gene signatures (*23*) previously shown to be positively correlated with survival in patients with HSV-1 seropositivity treated with CAN-3110 (*16*). Whereas DFCI1 had too few samples for meaningful statistical analyses, 11 of the 13 signatures in DFCI2 had positive correlations [false discovery rate (FDR) < 0.2] with the biopsy distance from the prior CAN-3110 tumor injection site (Fig. 2E), suggesting a localized impact of therapy on these signatures. The immune impact of CAN-3110 treatment was confirmed by CyCIF staining of immune cell subpopulations, revealing increases in $CD45^+$ leukocytes, $CD163^+$ macrophages, and $CD8^+$ T cells after therapy for both patients (Fig. 2F, fig. S3, and table S3). These results suggest that both patients had growing lesions with low tumor cellularity and increasing inflammation after treatment with CAN-3110, with lower tumor content and higher immune gene signature scores nearer to sites of CAN-3110 injection.

Longitudinal impact of CAN-3110 therapy was observed in global proteomic signatures

To further understand changes in the TME after therapy, we performed overall proteome (figs. S6 and S7) and concomitant gene expression analyses. Longitudinal changes in multiple proteins assayed were observed at each time point (figs. S6 and S7). For DFCI1, the posttrial craniotomy proteome appeared similar to the initial proteome (fig. S6A), whereas the proteomic changes for DFCI2 followed a different trajectory, with larger changes at 15 and 30 days followed by smaller changes at other time points (fig. S7A). Hierarchical clustering of the temporal proteomic changes resulted in multiple coregulated clusters (figs. S6B and S7B); temporal trajectories (figs. S6C and S7C) and biological processes (figs. S6D and S7D) represented by each of these clusters are provided. Most of these processes were related to metabolism, cellular transport signals, inflammation, and host responses to pathogens. There were multiple serial changes in the Hallmark gene signatures (fig. S8).

Longitudinal changes were observed in the GBM global phosphopeptidome during CAN-3110 treatment

Next, we analyzed the temporal evolution of proteins with phosphorylated serine, threonine, and tyrosine in the serial biopsies obtained from each patient during the successive injections with CAN-3110 (figs. S9 and S10). Dynamic changes in phosphorylated proteins were also detected for both patients, following relatively similar trajectories (fig. S10A). Peptides with coregulated changes clustered into seven or nine clusters for DFCI1 or DFCI2, respectively (fig. S10B); temporal trajectories for each cluster are presented in fig. S10C. We identified signaling pathways or processes where at least one of the biopsies revealed a change that was significant with an FDR less than or equal to 0.05 (fig. S9). Several of the genes in identified pathways have been implicated in tumor proliferation, such as *MAPK1*, *EGFR*, *CDK1*, and *CK2A1*.

Longitudinal changes in the GBM immunopeptidome were observed during serial CAN-3110 injections

GBM is known to have reduced HLA expression (*24*), a factor thought to be responsible for immunoevasion likely because of reduced presentation of immunopeptides. The gene expression and phosphoproteomic change led us to ask whether there was longitudinal evidence of changes in HLA expression with the expression of novel immunopeptides. The measured HLA-A, HLA-B, HLA-C, and HLA-DR expression levels were above the day 0 pretreatment baseline for nearly all biopsies collected after day 0 (Fig. 3A). Next, we screened for immunopeptides, and similar to HLA expression, HLA-I–bound immunopeptide representation was higher than the day 0 baseline in nearly all post–CAN-3110 biopsies for both patients, with nine-nucleotide oligomer immunopeptides predominating and select proteins, such as interferon-α inducible protein 6 (IFI6) and glial fibrillary acidic protein (GFAP), being most represented in the immunopeptidome (Fig. 3B and fig. S11). Several up-regulated immunopeptides belonged to previously identified pan-cancer cancer testis antigens (CTAs) and glioma-associated testis-specific antigens (Fig. 3C) (*25*–*29*). Further, receptor tyrosine kinase signaling, interferon responses, and apoptosis pathways were significantly (FDR < 0.05) up-regulated at numerous post–CAN-3110 time points relative to day 0 in both patients, supporting a temporal response to treatment (Fig. 3D). In addition, identified HLA-bound peptides (fig. S11, B to F) are known to be present in both glia and tumors (such as GFAP and myelin basic protein) (*30*), and some have been associated with GBM progression and invasion (such as VIM and S100A9) (*30*–*38*). The sum of these results thus indicated that the serial biopsy/injection procedures did increase immune activation signatures and HLA-immunopeptidome expression, with some of these being known glioma-associated CTAs and tumor-associated antigens.

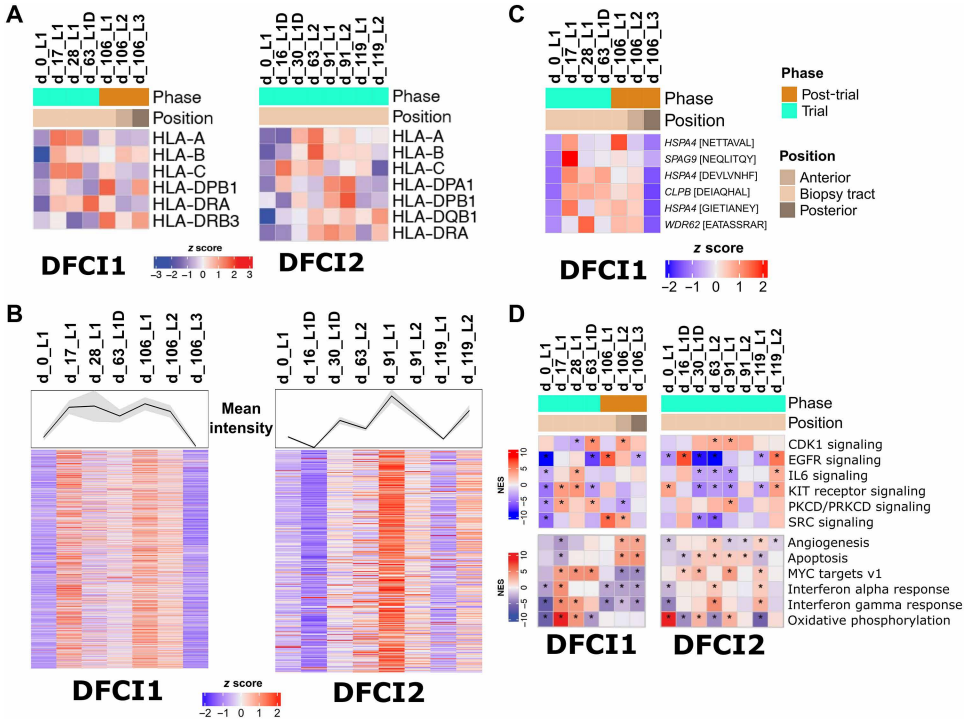

Fig. 3. HLA expression and immunopeptide abundance were increased posttreatment. (**A**) Heatmap of longitudinal changes in the expression of HLA-A, HLA-B, HLA-C, and HLA-DR proteins. The *z*-score represents a normalized scale for the expression of each HLA protein measured across the samples, with the spectrum from blue to red indicating lowest to highest expression. (**B**) Heatmap of longitudinal changes in HLA-I immunopeptides, with each row in the heatmap representing an individual immunopeptide. Mean intensity across all HLA-I immunopeptides with shaded SEM is plotted above each heatmap. (**C**) HLA-I ligands identified that were previously reported as CTAs and testis-specific antigens. The gene name of each antigen and its epitope detected (in parentheses) are indicated to the right of the heatmap. (**D**) Heatmap of longitudinal changes in select Hallmark signatures (top; collection of genes that define biological states or processes from the Molecular Signature Database) and signaling signatures (bottom; phosphorylation site-specific signatures from the Post-Translational Modification Signature Database) that were enriched, as assessed by proteomic/phospho-proteomic ssGSEA (v2.0) (top) and PTM-SEA (bottom) (*63*–*65*). The * inside each box denotes those with an FDR-adjusted $P \leq 0.05$. NES (normalized enrichment score) measures the magnitude of enrichment of each signature (indicated on the right) for each sample (red: highest, blue: lowest).

Longitudinal scRNA-seq revealed dynamic immune population changes after CAN-3110 therapy

CAN-3110's impact on immune populations was further assessed using scRNA-seq. Immune cells in tumors were clustered into T/natural killer (NK), myeloid, B, and plasma cells (fig. S12A). Analyses of the serial changes in GBMs showed that the proportion of cells changed with time. The baseline TME primarily consisted of nonimmune cells, presumably tumor and glial cells with a minimal presence of immune cells, consistent with the immunologically "cold" classification of GBM (*39*). The TME changed substantially over each injection and biopsy time point, and by the day 60 to 90 time points, more than 90% of the TME was composed of immune cells, including T cells, plasma cells, and myeloid cells (fig. S12, B to E).

We identified 25 clusters of T and NK cells in the rGBM biopsies (Fig. 4, A to C). Tumor effector T cells (T_{eff} cells; $IFNG^+LAG3^+CD8^+$, $GZMK^+IFNG^+CD8^+$, and $PDCD1^+CTLA4^+CD4^+$ T_{eff} cells) were observed at higher than baseline frequencies at nearly all posttreatment time points for both patients (Fig. 4B), with expansion of novel (not detected at baseline) T cell clonotypes and contraction of several preexisting T cell clonotypes during the longitudinal trial (Fig. 4, D and E). These results indicated that the serially treated rGBMs were infiltrated with activated $CD4^+$ and $CD8^+$ T_{eff} cells, suggesting an ongoing immunologic response.

The proportion of plasma cells also increased with time, and these cells also exhibited a transcriptional signature (*CD79A*, *MZB1*, *XBP1*, *CD38*, *CD27*, *IGHG1*, and *JCHAIN*) characteristic not only of maturation and antibody production but also of antigen presentation (fig. S12F) (*40*–*46*). The baseline GBM TME was also highly infiltrated with myeloid cells, including tumor-associated microglia, monocytes, and macrophages (fig. S13A) (*47*–*50*). Complex and dynamic shifts in multiple myeloid cell subpopulations occurred during the longitudinal biopsies and CAN-3110 injections (fig. S13, B and C). These shifts occurred with both immune-active M1 myeloid cells (fig. S13, D to F) and immunosuppressive M2 myeloid cells (fig. S13, G to I). Together, the longitudinal single-cell RNA analyses showed that the serial CAN-3110 injection changed the baseline TME with increases in immune-active plasma cells and T_{eff} cell clonotypes and complex changes in the myeloid cell population, where a baseline of immunosuppressive M2 cells became more infiltrated with immune-active M1 cells, including cDC1 cells.

HSV-reactive T cells were observed in rGBM biopsies after therapy

To characterize the T cell responses observed posttherapy, 96 T cell receptor (TCR) α/β chain pairs from the most expanded T cell clonotypes identified from single-cell TCR sequencing were reconstructed and screened for antigen specificity. In total, 192 TCRα/β pairs from 169 TCR clonotypes ($n = 83$ and $n = 86$ from DFC1 and DFCI2, respectively) were cloned and expressed using a lentiviral vector in healthy donor T cells using our established protocol (*51*). The reactivity mediated by each TCR was measured on TCR-transduced T cells as CD137 surface up-regulation after stimulation with patients' autologous Epstein-Barr virus (EBV)–immortalized lymphoblastoid cell lines (EBV-LCLs) pulsed with viral lysates from the oncolytic rQNestin34.5v.1 (a preclinical strain of CAN-3110), common viruses, or with overlapping peptide pools encoding for immunogenic epitopes from cytomegalovirus (CMV), EBV, influenza virus (Flu), and HSV1/2. A representative screen is shown in fig. S14A. We detected, for example, 31 TCRs (DFCI1: $n = 9$; DFCI2: $n = 22$) with specificity to CMV or EBV epitopes (fig. S14B). The

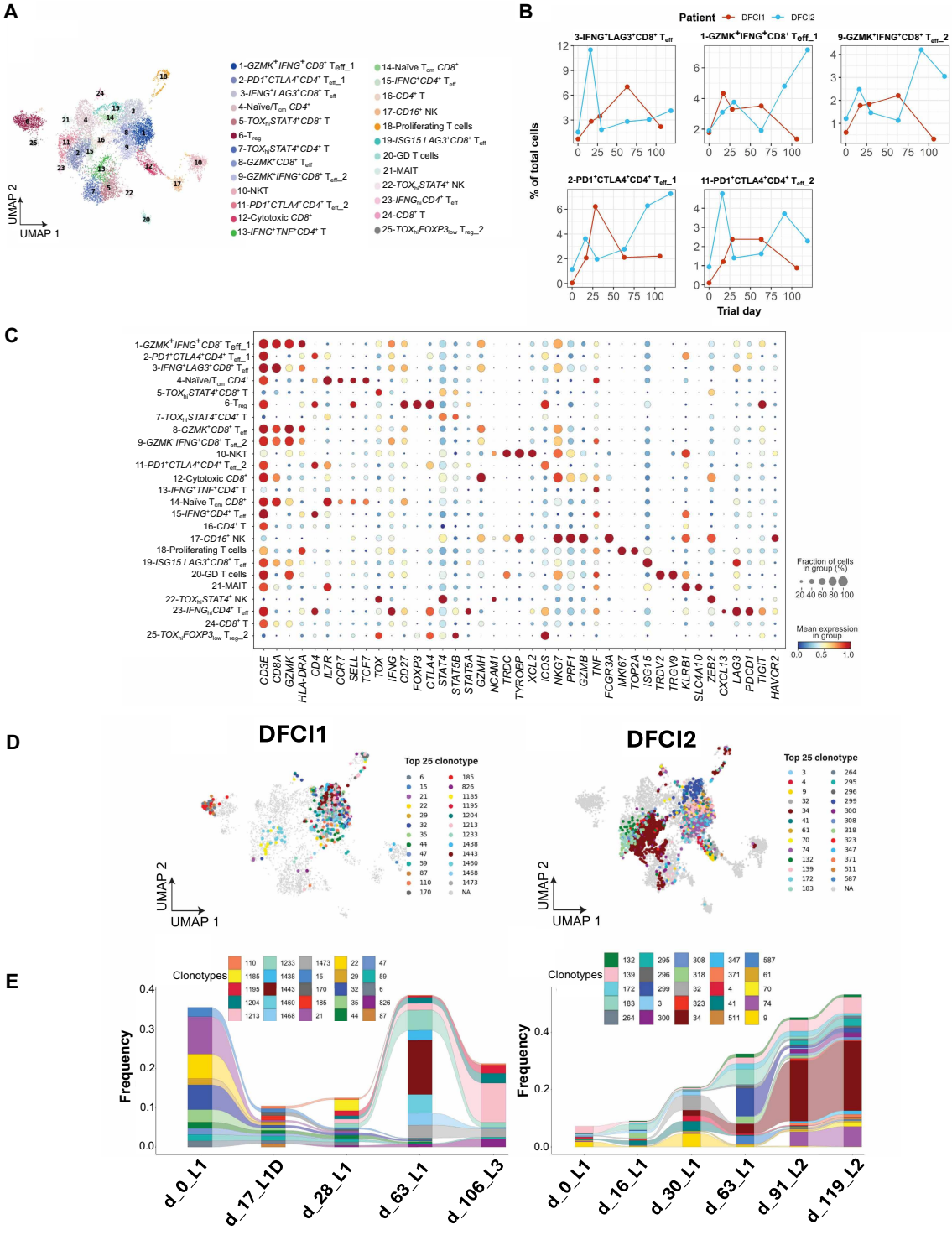

Fig. 4. T_{eff} cell frequencies increased posttherapy. (**A**) Uniform Manifold Approximation and Projection (UMAP) showing T and NK cell subclusters from scRNA-seq analysis. (**B**) Longitudinal changes in tumor T_{eff} cell populations (*IFNG*$^+$*LAG3*$^+$*CD8*$^+$ T_{eff} cells, *GZMK*$^+$*IFNG*$^+$*CD8*$^+$ T_{eff} cells, and *PDCD1*$^+$*CTLA4*$^+$*CD4*$^+$ T_{eff} cells) in DFIC1 (in red) and DFCI2 (in blue). (**C**) Dot plot showing marker gene expression for NK and T cell clusters as shown in (A) and (B). (**D**) Phenotypic distribution of top 25 T cell clones in DFCI1 (left) and DFCI2 (right). (**E**) Alluvial plot showing flux of each clone at each time point in DFCI1 (left) and DFCI2 (right). The second and third biopsies were allocated for scRNA-seq as shown in Fig. 1B. The biopsy locations used in the analyses are shown in the *x*-axis labels of (E).

screening resulted in the identification of 50 TCRs (DFCI1: $n = 25$; DFCI2: $n = 25$) with reactivity to rQnestin34.5 v.1/CAN-3110 and/or to HSV lysates or proteins (HSV/rQNestin34.5v.1/CAN-3110–reactive TCRs; Fig. 5A and fig. S14C). The analysis of single-cell profiles of tumor-infiltrating lymphocytes (TILs) harboring CD8-restricted HSV/CAN-3110–reactive TCRs (16 clonotypes) revealed an enrichment (FDR < 0.2) in *IFNG*$^+$*LAG3*$^+$*CD8*$^+$ T_{eff} cells in both DFCI1 and DFCI2. Similarly, TILs with CD4-restricted HSV/CAN-3110–reactive TCRs (34 clonotypes) were enriched (FDR < 0.2) among *PDCD1*$^+$*CTLA4*$^+$*CD4*$^+$ T_{eff} cells in DFCI2, although no significant enrichment was observed for DFCI1 (Fig. 5B and fig. S15, A to D). *CD8*$^+$ HSV/CAN-3110–reactive TILs displayed a tissue-resident transcriptional program driven by the up-regulation of the Hobit (*ZNF683*) transcription factor (*52*–*56*) and characterized by an activated profile that lacked expression of *TOX*, a marker of terminal exhaustion (Fig. 5C). In addition, none of the *CD4*$^+$ HSV/CAN-3110–reactive TILs exhibited an immunosuppressive *FOXP3*$^+$ regulatory T cell profile (fig. S15D).

No HSV/CAN-3110–reactive TILs in biopsies from DFCI1 or DFCI2 were detected at the day 0 time point, but the abundance of these cells significantly increased over time ($P = 0.039$ and $P = 0.011$ for DFCI1 and DFCI2, respectively), eventually making up more than 15 and 30% of intratumoral T cells for DFCI1 and DFCI2, respectively (Fig. 5D). When analyzed in combination with radiographic imaging, HSV/CAN-3110–reactive T cells were largely restricted to biopsies taken within enhancing regions of the tumor, particularly in DFCI2, who was HSV1 seropositive (Fig. 5E). HSV/CAN-3110–reactive T cell frequency was nominally correlated with distance from prior CAN-3110 injection sites for CD4$^+$ but not for CD8$^+$ T cells (Fig. 5F). The lack of spatial constraint for the CD8$^+$ T cells may reflect their migratory abilities, with the distribution of CD4$^+$ T cells being possibly related to lower HLA-II expression near CAN-3110 tumor injection sites (Fig. 5G). These results demonstrate that CAN-3110 treatment elicits CD4$^+$ and CD8$^+$ HSV/CAN-3110–reactive T_{eff} cells with spatially defined distributions according to MRI enhancement and distance from virus injection. These data also show that the activity of CAN-3110 is specific, given that presumed bystander T cells (anti-CMV/EBV) do not show increased abundance or evidence of specific spatial localization. Together, the data from these first two patients reveal that longitudinal intratumoral CAN-3110 treatment leads to temporal changes in tumor density, GBM tumor cell states, immune activation signatures, immunopeptides, anti-HSV T cells, and MRI enhancement. It also leads to spatial changes in tumor density, HLA-II proteins, anti-HSV T cells, and immune signatures (fig. S16).

DISCUSSION

Confirmation of adequate pharmacokinetic exposure and pharmacodynamic effects in the tumor at serial, defined time points during therapy has not been routinely performed for GBM. We hypothesized that the convergence of modern neurosurgical technology with sophisticated multiomic molecular analysis (*15*) would allow for safe and informative longitudinal tumor sampling during oncolytic CAN-3110 immunotherapy, successfully capturing the cellular and molecular responses in the rGBM undergoing an applied immune perturbation. We hypothesized that integrative analyses of multiomic data from longitudinal planned tumor biopsies would critically aid interpretation of serial MRI changes, which are the historical benchmark for response assessment in this disease. As proof of concept, data on biopsies collected from the first two trial participants showed that (i) longitudinal GBM sampling is feasible and that patients can tolerate multiple serial tumor biopsy procedures; (ii) multiomic profiling provides insights into GBM response to CAN-3110 that was missed by routine imaging and pathology; and (iii) dense longitudinal sampling found spatial and temporal relationships between treatment and disease with just two patients, although these relationships were not apparent in our previous trial of 41 patients with less robust tissue collection (*16*). Serial biopsies also suggested that (i) decreased tumor content spatially correlated with distance from treatment site and a shift in tumor phenotype and increased inflammation after therapy; (ii) immune signatures previously shown to be correlated with survival in patients treated with CAN-3110 (*16*) were spatially related to distance from treatment location; (iii) up-regulation of immunopeptides, some of which have been described as CTAs and glioma-associated testis antigens, occurred after CAN-3110 administration along with proteomic pathways associated with immune activation; and (iv) treatment-reactive T cells increased posttherapy with spatially defined distributions not observed in bystander T cells, with expression of the gene encoding Hobit, known to be associated with tissue-resident memory-like T_{eff} cells and with responses to immunotherapy (*52*–*56*).

Between 5 and 13 tumor biopsy cores were collected from between one and three locations along one or two needle tracks at each planned time point for each patient. In both patients, serial gadolinium-enhanced MRI results were consistent with tumor recurrence during the trial (*17*–*19*). However, multiomic analyses of the GBM biopsies showed predominantly immune alterations in the TME, rather than tumor recurrence. These results indicate a discordance between MRI response assessment of tumor progression (*57*) and biopsy results consistent with reactive changes and diminished tumor, underscoring that MRI criteria may be limited or even misleading in the evaluation of investigational therapies such as immunotherapies.

Patient 1 was only 4 months from radiation therapy, and the initial biopsy before CAN-3110 injection showed evidence of radiation therapy–induced changes (necrosis with few tumor cells), and an MRI scan showed increased enhancement as compared with previous MRI scans. However, during the CAN-3110 serial clinical trial, as the enhancement in the MRI increased, one routine and customary interpretation would be progression or radiation-induced pseudoprogression and, consequently, CAN-3110 therapy failure. Instead, the multiomic analyses of the serial biopsies showed that the increased observed enhancement was likely due to the CAN-3110–elicited inflammatory and immune changes rather than to the traditional interpretation of tumor progression or radiation therapy–induced pseudoprogression.

Multiomic analyses of the longitudinal biopsies showed intratumoral enrichment of T cells that may establish immunological memory, where T cells underwent clonal expansion coupled with up-regulation of HLA immunopeptidomes, some of which were identified as known CTAs and glioma-associated testis antigens (*25*–*29*). Among these HLA-I peptides, CTAs are particularly important for tumor immunogenicity (*58*). Their expression in GBM has been well documented and is linked to improved prognosis (*26*, *59*, *60*). CTAs offer a unique advantage in cancer immunotherapy because they are typically lowly expressed in healthy tissues while

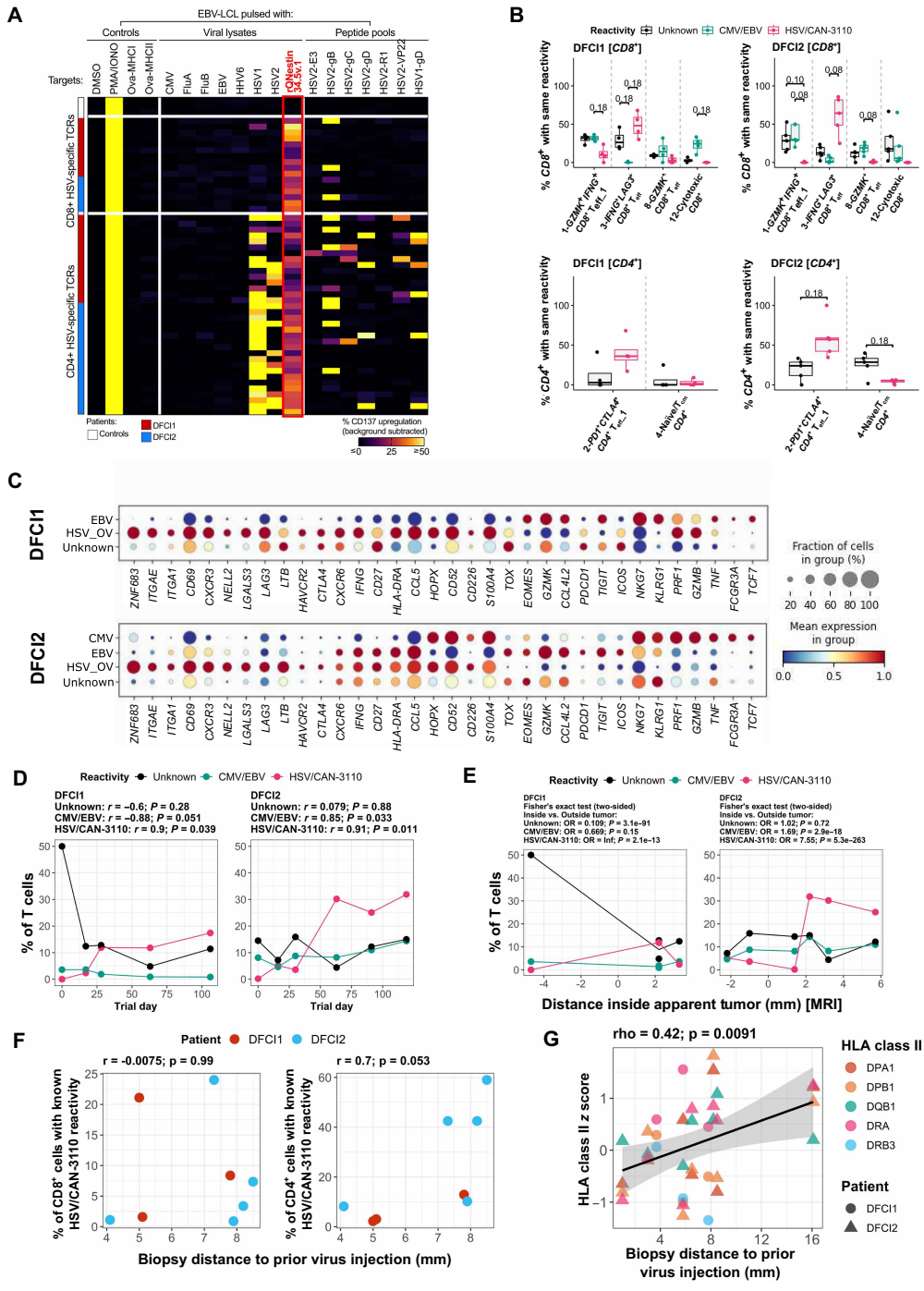

Fig. 5. HSV/CAN-3110–reactive T cells are present in the tumor with increasing frequency over time. (**A**) Heatmap showing reactivities of TCRs identified as HSV/CAN-3110 reactive. CD137 up-regulation was measured on TCR-transduced (mTRBC$^+$) CD8$^+$ or CD8$^-$(CD4$^+$) T cells cultured with autologous B cells immortalized with EBV (EBV-LCLs) and pulsed with controls, viral lysates, or peptide pools from commercially available immunogenic HSV1-HSV2 proteins. Background detected on transduced T cells stimulated with dimethyl sulfoxide (DMSO)–pulsed EBV-LCLs was subtracted. Left track: Patients'TCRs were divided on the basis of detection among CD4$^+$ or CD8$^+$ T cells (from scRNA-seq). Control TCRs: untransduced cells ($n = 1$) or T cells transduced with irrelevant TCRs ($n = 2$). rQnestin34.5v.1 is a precursor to rQnestin34.5v.2 (CAN-3110) (*61*, *66*). (**B**) Box plots show T cell cluster frequencies for CD8$^+$ (top) and CD4$^+$ (bottom) T cells with known reactivities. *y*-axis values are plotted as a percentage of all T cells with the same experimentally determined reactivity [i.e., experimentally tested but with no determined specificity (unknown), CMV/EBV (CMV_EBV), or HSV/CAN-3110 (HSV_OV)]. FDR values from paired *t* tests are shown for all T and NK clusters where FDR ≤ 0.2 in at least one patient. Box plots for T and NK clusters with FDR > 0.2 are provided in fig. S15D. CMV/EBV-reactive clones were omitted from the CD4$^+$ plot, given that no CMV/EBV-reactive CD4 clones were identified in our study. (**C**) Marker gene expression for CD8 T cells with CMV, EBV, HSV/CAN-3110 (HSV_OV), or unknown reactivity for DFCI1 (left) and DFCI2 (right). (**D**) scRNA-seq–based T cell frequencies over time for DFCI1 (left) and DFCI2 (right) for T cells with varying reactivities. Odds ratios per day and *P* values are shown above each plot showing results for each reactivity group from logistic regression of T cell counts (reactive versus nonreactive) versus time. (**E**) scRNA-seq–based frequencies of varying T cell reactivities versus the distance each biopsy was taken within apparent tumor enhancement as observed in MRI. Two HSV1 points for DFCI1 are almost entirely overlapping at 2.2 mm and 12%. Odds ratios and *P* values are shown above each plot for Fisher's exact test (two-sided) assessment for each reactivity for a difference in reactive versus nonreactive T cell counts in combined samples outside apparent tumor ($x < 0$) versus combined samples inside apparent tumor ($x > 0$). (**F**) Frequency of HSV1/CAN-3110–reactive CD8 (left) or CD4 (right) T cells versus the distance each biopsy was collected from the nearest prior CAN-3110 injection site. *r* and *P* values are from Pearson's correlation. (**G**) Scatterplot of expression of HLA-II (-DR) proteins from proteomic profiling (*z*-scores calculated across all assayed samples on a per-patient basis) versus distance from biopsy site to nearest prior CAN-3110 injection site. A linear regression trend line is shown with the shaded area representing the *t* distribution–based 95% confidence interval of the mean. Spearman's correlation coefficient (rho) and *P* value are shown above the plot. Precise tissue locations could not be determined for the DFCI1 day 106 resection surgery, so this time point is missing from (E) to (G).

enhancing tumor immunogenicity. These findings suggest that inflammation induced by CAN-3110 through recruitment of HSV/CAN-3110–reactive TILs may also promote the release and presentation of tumor-specific (rather than viral-based) antigens; these antigens, in turn, might be targeted by tumor-reactive T cells. We also characterized the identity of T cell clonotypes reacting against HSV/CAN-3110 epitopes and showed their expansion as emergent clones in GBM. Although we could not detect reactivities to tumor (nonviral) epitopes among dominant intratumoral T cell clones, we speculate that such a response might remain subdominant compared with those elicited by CAN-3110 and might be elicited at later time points. Further studies on less abundant TCR clonotypes emerging after therapy are warranted to investigate the spreading of tumor antigens induced by CAN-3110 treatment. However, the finding of up-regulation of HLA-immunopeptides with emergent tumor T cell clonotypes suggests that there may be specific antitumor immunity occurring, perhaps suggesting the occurrence of epitope spreading as discussed below. Coupled with the clinical correlation of a marked pathologic response in patient 1 and durable stable disease without further treatment in patient 2, our findings suggest that serial CAN-3110 may be eliciting antitumor immunity.

The infiltration of HSV/CAN-3110–reactive $CD4^+$ and $CD8^+$ T cells, coupled with their spatial localization in the tumor, makes it likely that the observed cellular, immunologic, and molecular perturbations are a result of the serial CAN-3110 injections rather than a sham effect from repeated biopsy/injection injury to the tumor. In our previous report (*16*), we also showed that preexistent serology to HSV1 was associated with improved survival after CAN-3110 and with more viral clearance of injected tumors. Therefore, serial injections with CAN-3110 may increase the antitumor immune effect, perhaps through epitope spreading as HSV-reactive T cells and antibodies attempt to clear CAN-3110–infected tumor cells.

Integrating the multiomic analyses shows temporal and spatial differences in tumor and immunologic responses to CAN-3110. Temporally, there were increased immune activation signatures, immunopeptides, MES-like GBM cells, HSV/CAN-3110–reactive T cells, and MRI enhancement with decreased tumor density and AC-like GBM cells. Spatially, tumor density, HLA-II proteins, and HSV/CAN-3110–reactive $CD4^+$ T cells decreased with distance from the previous CAN-3110 injection site. Conversely, reduced HLA-I, M1 signatures, myeloid-derived suppressor cell trafficking, coactivation molecules, and $CD8^+$ T_{eff} cells increased with distance from the previous CAN-3110 injection site (fig. S16). This suggests that multiple locoregional administrations of CAN-3110 can reshape the TME of GBM lesions, eliciting beneficial antitumor immunity.

The implementation of serial biopsies and multiomic analyses into routine clinical practice could occur by striving for workflow processes and patient care paradigms where each biopsy becomes a same-day outpatient procedure, such as what is done for chemotherapy infusions. Each procedure would be performed under conscious sedation anesthesia, and the length of each procedure would be minimized to an hour or less for patient comfort, as we did in this trial. Although the integrated "omic" analyses were not part of clinical care or decision-making for this trial, if serial biopsies become accepted in the evaluation of current standard of care or experimental therapies, then the serial omic analyses will need to become clinically certified molecular tests, with results that are accessible in a time frame that allows for clinical decision-making, similar to genomic exome sequencing platforms being used today.

Limitations of this study are several. First, it only encompassed the first two patients in this trial, and it may not be reflective of the entire cohort of 12 patients planned for this trial. As of July 2025, 9 of the 12 patients have been accrued, and multiomic analyses of longitudinally collected rGBM, CSF, and blood samples before and after CAN-3110 are ongoing. Instead of waiting for the final analyses on all 12 patients, which is still a few years away, we argue that the current clinical feasibility and scientific data should be published now, although they only represent these first two patients. We hope that this study can launch a discourse on the value of longitudinal tissue sampling for GBM for current and future clinical trials, so that we can improve our understanding of investigational therapy effects. Second, there was evidence of heterogeneity in the biopsy samples at multiple time points and locations. However, the trajectory of longitudinal changes compared with the day 0 preinjection biopsy does suggest validity in the observed cellular and molecular analyses from CAN-3110 tumor injections. Third, although we used traditional MRI to follow patient outcomes, arguments could be made that additional imaging modalities based on positron emission tomography or other MRI sequences could help detect true progression from the inflammatory pseudoprogression observed in this trial. However, imaging modalities are unlikely to provide the detailed information obtained with the integrated multimodal omic analyses of cellular and molecular pathways possible with tumor tissue acquisition. Last, we have not reported on the longitudinal CSF and blood correlates, which will be the subject of future reports.

Overall, these findings illustrate that longitudinal tumor biopsies are safe and feasible for patients with GBM. Further, serial interrogation by longitudinal biopsy cores of rGBM during therapy uncovered therapeutic pharmacodynamic effects that could not be surmised by routine MRI or clinical analyses. The breadth and depth of data generated from analyses performed on longitudinal tumor biopsy cores underscore the value of this approach in the context of therapeutic drug delivery. However, overall biologic conclusions will require additional similar analyses among patients who continue to enroll in this trial. Our results provide impetus to adopt a previously unrecognized paradigm for GBM investigational drug development that incorporates longitudinal tumor sampling in clinical trials. Longitudinal sampling provides real-time assessments of tumor response to therapeutic perturbation over time. The number and schedule of longitudinal tumor biopsy core samplings in future studies should be based on the expected mechanism of action and pharmacokinetic features unique to each investigational agent. Investigational agents with evidence of intratumoral delivery and pharmacodynamic impact on the tumor based on longitudinal sampling should be prioritized for further clinical development over those that do not, thereby allowing precious clinical and patient resources to be committed to investigational agents with the greatest promise for patients with these devastating tumors.

MATERIALS AND METHODS

Study design

This was an open-ended, multi-institutional, unblinded, three-armed (arms A to C), dose-escalation phase 0/1 trial. The first arm of the trial (arm A) involved nine cohorts of participants ($n = 30$) treated in a three-plus-three dose-escalating design with CAN-3110 [formerly known as rQNestin34.5v.2 (*61*)] injected in a single area of tumor followed by a 10th cohort ($n = 12$) of patients treated with

one dose injected in two to five sites of the tumor. No dose-limiting toxicities (DLTs) were observed, and a maximum-tolerated dose (MTD) was not defined for a single time-point injection of CAN-3110 (*16*). A second, yet unpublished, arm (arm B) was assessed to test the safety of administration of cyclophosphamide as a single pre-immunomodulatory dose before injection of a single CAN-3110 dose of 10^8 or 10^9 plaque-forming units (PFUs) in nine participants.

The primary objective of arm C (present study of 2 of 12 total patients) was to determine the safety of up to six intratumoral repeated doses of rQNestin34.5v.2/CAN-3110, first in a cohort receiving 10^8 PFUs per time point, followed by a cohort receiving 10^7 PFUs per time point for cumulative doses of 6×10^8 or 6×10^7 PFUs. The secondary objectives for arm C were to assess the therapeutic benefit including overall survival (OS), progression-free survival, tumor objective response rate, and rate of pseudoprogression. Exploratory objectives were to assess (i) the longitudinal persistence of rQNestin34.5v.2 antigen, DNA, and transcripts in injected rGBM; (ii) the longitudinal changes in cellular, molecular, and immunologic variables in injected glioma; (iii) the longitudinal changes in blood biomarkers from injected glioma; (iv) the correlation of longitudinal changes in sampled glioma cellular, molecular, and immunologic variables with changes in peripheral biomarkers and CSF biomarkers via Ommaya; and (v) the spatial correlation of longitudinal MRI changes with anatomic biopsy and injection sites of rQNestin34.5v.2.

Arm C incorporated a Bayesian optimal interval (BOIN) design (*62*) in which the CAN-3110 dose was planned to be decreased to 1×10^7 PFUs per dose if the MTD was exceeded in the 1×10^8 PFU cohort and increased to 1×10^9 PFUs per dose if the MTD was not exceeded at the 1×10^8 PFUs per dose level. The BOIN design was used to adaptively guide both intrapatient dose escalation, which determined the number of repeat doses/injections that a patient can safely receive, and interpatient dose escalation between patient cohorts. The MTD was defined as the dose with the target DLT rate of 0.3, determined on the basis of the design recommendation using isotonic regression and the totality of the safety data. As part of the trial, an Ommaya reservoir was also placed in the frontal horn of the lateral ventricle during the day 0 procedure, and CSF was also obtained at each procedure. In addition, blood was collected before and after each procedure to isolate PBMCs. Both CSF and PBMC studies were planned to provide longitudinal peripheral biofluid correlations with the longitudinal stereotactic biopsies.

Regulatory approvals

This phase 1 clinical trial was approved by the National Institutes of Health (NIH) Recombinant DNA Advisory Committee (RAC) Office of Biotechnology Affairs (NIH no. 1104-1100) and the Dana-Farber Harvard Comprehensive Cancer Center Institutional Review Board (IRB) (no. 16-557). It was sponsored under Investigational New Drug (IND) no. 16380 [E.A.C., Brigham and Women's Hospital (BWH), Boston, MA].

Patient characteristics

DFCI1 was a 54-year-old right-handed Caucasian male with a history of a gross total resection of a right frontal GBM, *IDH* wild type [*MGMT* promoter partially methylated; point mutations *TERT*, *TP53*, and *PIK3CB*; tumor mutational burden (TMB), 1.2 Mb] after a presentation of progressive headaches. He underwent standard radiation therapy with daily temozolomide followed by four cycles of adjuvant temozolomide, at which point radiographic tumor progression was documented. Progression diagnosis occurred 7 months from his initial surgery and nearly 4 months from completion of radiation therapy. The patient was neurologically intact at that time and enrolled in the longitudinal CAN-3110 trial. Stereotactic biopsy at study enrollment confirmed infiltrating GBM, and the study therapy was initiated. The time course and dose of CAN-3110 and relevant findings at each study time point are summarized in table S4. Three days after his baseline CAN-3110 injection, he developed a fever to 38.8°C accompanied by nausea and chills. No source of the fever was identified, and his symptoms resolved within 24 hours. As noted in table S4, he remained neurologically intact throughout the course of study treatment except for mild subjective left-hand weakness, which developed after procedure 3 (day 30) and resolved with five doses of tapering dexamethasone over 3 days (4 mg for first day, 2 mg for second, and 1 mg for days 3 to 5). The patient was treated once more with a short course of dexamethasone on day 78 to day 80. The day before the fifth study procedure (day 90), the patient elected to withdraw from the study because of concern of possible tumor progression based on MRI findings at that time. He underwent an elective craniotomy with resection of the enhancing material noted on brain MRI (data file S1) at the day 100 time point. Histopathologic review revealed predominantly inflammation, immune infiltration, and evolving gliosis with no clear evidence of tumor recurrence (data file S1).

DFCI2 was a 66-year-old right-handed female with a history of germline *BRCA1* mutation, estrogen receptor/progesterone receptor (ER/PR) negative, $Her2^+$ breast cancer (previously treated and disease-free) who underwent a gross total resection of a ring-enhancing left occipital GBM *IDH* wild type [*MGMT* promoter unmethylated; with epidermal growth factor receptor (EGFR) focal amplification; two-copy loss *CDKN2A/B*; TMB 1.8/MB] after a presentation of progressive expressive aphasia and a right homonymous hemianopsia. She underwent standard radiation with concurrent temozolomide over 6 weeks followed by adjuvant temozolomide for six cycles. Twenty-one months after completing adjuvant temozolomide, she developed radiographic progression, at which point her baseline expressive aphasia and homonymous hemianopsia were stable. She enrolled in the longitudinal CAN-3110 trial and underwent a stereotactic biopsy confirming infiltrating GBM (data file S1). The time course and dose of CAN-3110 and relevant findings at each study time point are summarized in table S5. Throughout the study, her baseline neurologic deficits persisted, and she developed subjective, mild right-sided weakness after dose 3, which improved with a 3-day dexamethasone pulse, but nonetheless has persisted. At the time of the preparation of this report, DFCI2 has fully completed the study therapy. However, there was continued enhancement with some slight increase with evolution of her clinical picture: Although independent, by 18 months, serial MRI scans showed new enhancement across the splenium with clinical evolution of a right hemiparesis and increased dysphasia (data file S1). Treatment with dexamethasone, bevacizumab, and niraparib was initiated. She remains alive at 24 months.

Informed consent

Each patient signed a standard Brigham and Women's Hospital (BWH) informed consent form for clinical procedure for each stereotactic biopsy and then a protocol-specific research consent form for injection of the investigational agent [DFCI protocol number 16/557, principal investigator (PI): E.A.C., BWH, and Mass General Brigham]

and for the collection and scientific analyses of each biopsied GBM core (DFCI protocol number 10/417, PI: K.L.L., BWH/DFCI). Each of these three consents was reaffirmed before each of the planned procedures on days 0, 15, 30, 60, 90, and 120. Subsequently each of the two patients in this trial signed a separate BWH consent for public release and deidentification of their personal health information (PHI) data for this publication and other possible public disclosures.

Eligibility criteria

The size of the enhancing component of the tumor had to be ≥1 cm to allow both a tumor size that could be biopsied at one site and injected at a different site. The initial tumor had to be ≤2 cm in greatest maximal diameter and located in either the nondominant cortex or in the occipital dominant cortex to maximize patient safety while allowing for the six time-point injections over 4 months. The tumor was also required to be sufficiently far from the functional cortex defined as sensorimotor and speech centers and associated fiber tracts to allow for anticipated completion of the serial treatments over 4 months as judged by the treatment team. Patients were required to have a Karnofsky performance score of at least 70, adequate organ function, no dexamethasone therapy within 14 days of study therapy initiation, and no prior anti-angiogenic therapy including bevacizumab.

AE grading

Adverse events (AEs) were graded on the basis of CTCAE v5.0 criteria. The determination of attribution was complex in this setting because these could be due to CAN-3110, to the longitudinal multiple surgical procedures, or to the natural course of disease. Within the protocol, several scenarios were provided to aid each principal investigator and the sponsor in considering factors that would allow attribution to one or a combination of etiologies.

Neurosurgical technical notes

Each intervention for the two patients reported here was carried out in the operating room as an outpatient procedure at BWH. Patients underwent conscious and not general anesthesia, with local anesthesia applied for skull fixation and scalp incision. The frameless stereotactic apparatus was the Navigus device with Stealth navigation stations (Medtronic Inc.). Biopsy site(s) and injection sites were preidentified before each procedure, ensuring that the latter was in a separate area of tumor. Biopsy sites were selected to be close to the previous treatment injection site for subsequent procedures (days 15, 30, 60, 90, and 120). Surgical planning for biopsy sites and injection sites was reviewed preoperatively by the site PIs using an app-based platform (Acesis Inc.). CSF was obtained from the Ommaya catheter after each tumor biopsy and treatment administration to avoid brain shifts that could hamper the precision of the intraoperative biopsy and injection. In addition, diuretics (mannitol, Lasix) and corticosteroids were not administered unless medically necessitated, and the patient's head was left in a horizontal position without the customary head elevation to minimize brain shift. No hemostatic material (gelfoam, surgicel) was placed in the used burr hole at each injection to minimize the amount of absorbable foreign material that could harbor bacteria. A single layer of interrupted vertical mattress sutures was used to close the skin without a separate layer of galea sutures. These sutures were removed in a sterile manner in the operating room at the day 15 and day 30 time points, whereas sutures at subsequent time points were removed in the office. A postoperative MRI scan was obtained within 6 hours to allow determination of the anatomical sites for each biopsy and for each injection.

For both patients in this report, each dose of CAN-3110 was 1×10^8 PFUs reconstituted in 1 or 2 ml (based on number of injections in tumor) of sterile saline and injected through the SmartFlow (MRI Interventions Inc.) cannula by hand over ~5 min. The dose at each time point was administered to a single intratumoral location except for the day 0 dose for DFCI2, which was equally divided between two intratumoral locations (0.5×10^8 PFUs in 1 ml each). The injection catheter was left in place upon completion of the injection for 5 min before being removed.

Biopsy site names

Each individual biopsy site location (d_63_L1, d_63_L1D, d_63_L2, etc.) reflects a single biopsy needle position at which multiple biopsy cores may have been collected. For a site named d_63_L1, the biopsy would have been collected at trial day 63 in location 1 for that surgery. Note that location names are specific to each surgery and are not conserved across time points (L1 in the first surgery may not be related to L1 in the second surgery, etc.). If the biopsy needle was moved to a deeper depth along the same needle track, then the difference in location was denoted by appending "D" to the prior location (if day 63 cores were taken at one location, then the needle was inserted farther and additional cores were collected; the first location would be d_63_L1 and the second location would be d_63_L1D). If cores were collected from a different biopsy needle track, then a new location name was used (d_63_L2).

Statistical analysis

For assays on biopsy core tissue, technical replicates were not performed unless otherwise noted in figure legends. For TCR specificity screening, two or three technical replicates were performed for each negative control and HSV/CAN-3110 response condition on the basis of the availability of stimulating reagents, with other conditions being performed in singlet. For analyses involving statistical tests, each test is noted in the figure legend. All tests were two sided. For correlative analyses, Pearson's correlation *P* values (two-sided, based on *t* distribution) or Spearman's correlation *P* values (two-sided, based on *t* distribution) were calculated on the basis of appearance of data as having a linear or nonlinear trend. Spearman's correlation tests were also performed where variables violated the bivariate normality required for Pearson's correlation tests. For Pearson's correlation analyses, the violation of bivariate normality was tested using the Henze-Zirkler's test. For *t* tests, normality was tested using the Shapiro-Wilk test, and any comparisons with significant deviation from normality (FDR < 0.1) were discarded. For immunopeptidomic enrichment analyses, the default test (Fisher's exact test) for the Enrichr analysis software was used. All individual-level tabular data are presented in data file S2.

Supplementary Materials

The PDF file includes:

Methods
Figs. S1 to S16
Tables S1 to S5
Legends for movies S1 and S2
Legends for data files S1 and S2
References (*67*–*86*)

Other Supplementary Material for this manuscript includes the following:
Movies S1 and S2
Data files S1 and S2
MDAR Reproducibility Checklist

REFERENCES AND NOTES

1. L. R. Schaff, I. K. Mellinghoff, Glioblastoma and other primary brain malignancies in adults: A review. *JAMA* **329**, 574–587 (2023).
2. M. A. Vaz-Salgado, M. Villamayor, V. Albarran, V. Alia, P. Sotoca, J. Chamorro, D. Rosero, A. M. Barrill, M. Martin, E. Fernandez, J. A. Gutierrez, L. M. Rojas-Medina, L. Ley, Recurrent glioblastoma: A review of the treatment options. *Cancer* **15**, 4279 (2023).
3. N. S. Cho, W. K. Wong, P. L. Nghiemphu, T. F. Cloughesy, B. M. Ellingson, The future glioblastoma clinical trials landscape: Early phase 0, window of opportunity, and adaptive phase I-III studies. *Curr. Oncol. Rep.* **25**, 1047–1055 (2023).
4. G. R. Harsh, T. S. Deisboeck, D. N. Louis, J. Hilton, M. Colvin, J. S. Silver, N. H. Qureshi, J. Kracher, D. Finkelstein, E. A. Chiocca, F. H. Hochberg, Thymidine kinase activation of ganciclovir in recurrent malignant gliomas: A gene-marking and neuropathological study. *J. Neurosurg.* **92**, 804–811 (2000).
5. F. F. Lang, M. R. Gilbert, V. K. Puduvalli, J. Weinberg, V. A. Levin, W. K. Yung, R. Sawaya, G. N. Fuller, C. A. Conrad, Toward better early-phase brain tumor clinical trials: A reappraisal of current methods and proposals for future strategies. *Neuro Oncol.* **4**, 268–277 (2002).
6. F. F. Lang, C. Conrad, C. Gomez-Manzano, W. K. A. Yung, R. Sawaya, J. S. Weinberg, S. S. Prabhu, G. Rao, G. N. Fuller, K. D. Aldape, J. Gumin, L. M. Vence, I. Wistuba, J. Rodriguez-Canales, P. A. Villalobos, C. M. F. Dirven, S. Tejada, R. D. Valle, M. M. Alonso, B. Ewald, J. J. Peterkin, F. Tufaro, J. Fueyo, Phase I study of DNX-2401 (delta-24-RGD) oncolytic adenovirus: Replication and immunotherapeutic effects in recurrent malignant glioma. *J. Clin. Oncol.* **36**, 1419–1427 (2018).
7. J. M. Markert, P. G. Liechty, W. Wang, S. Gaston, E. Braz, M. Karrasch, L. B. Nabors, M. Markiewicz, A. D. Lakeman, C. A. Palmer, J. N. Parker, R. J. Whitley, G. Y. Gillespie, Phase Ib trial of mutant herpes simplex virus G207 inoculated Pre-and post-tumor resection for recurrent GBM. *Mol. Ther.* **17**, 199–207 (2009).
8. P. Y. Wen, M. Touat, B. M. Alexander, I. K. Mellinghoff, S. Ramkissoon, C. S. McCluskey, K. Pelton, S. Haidar, S. S. Basu, S. C. Gaffey, L. E. Brown, J. E. Martinez-Ledesma, S. Wu, J. Kim, W. Wei, M. A. Park, J. T. Huse, J. G. Kuhn, M. L. Rinne, H. Colman, N. Y. R. Agar, A. M. Omuro, L. M. DeAngelis, M. R. Gilbert, J. F. de Groot, T. F. Cloughesy, A. S. Chi, T. M. Roberts, J. J. Zhao, E. Q. Lee, L. Nayak, J. R. Heath, L. L. Horky, T. T. Batchelor, R. Beroukhim, S. M. Chang, A. H. Ligon, I. F. Dunn, D. Koul, G. S. Young, M. D. Prados, D. A. Reardon, W. K. A. Yung, K. L. Ligon, Buparlisib in patients with recurrent glioblastoma harboring phosphatidylinositol 3-kinase pathway activation: An open-label, multicenter, multi-arm, phase II trial. *J. Clin. Oncol.* **37**, 741–750 (2019).
9. E. Chen, A. L. Ling, D. A. Reardon, E. A. Chiocca, Lessons learned from phase 3 trials of immunotherapy for glioblastoma: Time for longitudinal sampling? *Neuro Oncol.* **26**, 211–225 (2024).
10. J. D. Christie, E. A. Chiocca, Treat and repeat: Oncolytic virus therapy for brain cancer. *Nat. Med.* **28**, 1540–1542 (2022).
11. T. Todo, H. Ito, Y. Ino, H. Ohtsu, Y. Ota, J. Shibahara, M. Tanaka, Intratumoral oncolytic herpes virus G47Δ for residual or recurrent glioblastoma: A phase 2 trial. *Nat. Med.* **28**, 1630–1639 (2022).
12. K. Singh, K. M. Hotchkiss, I. F. Parney, J. De Groot, S. Sahebjam, N. Sanai, M. Platten, E. Galanis, M. Lim, P. Y. Wen, G. Minniti, H. Colman, T. F. Cloughesy, M. P. Mehta, M. Geurts, I. Arrillaga-Romany, A. Desjardins, K. Tanner, S. Short, D. Arons, E. Duke, W. Wick, S. J. Bagley, D. M. Ashley, P. Kumthekar, R. Verhaak, A. J. Chalmers, A. P. Patel, C. Watts, P. E. Fecci, T. T. Batchelor, M. Weller, M. A. Vogelbaum, M. Preusser, M. S. Berger, M. Khasraw, Correcting the drug development paradigm for glioblastoma requires serial tissue sampling. *Nat. Med.* **29**, 2402–2405 (2023).
13. M. M. J. Bauman, S. M. Bouchal, D. D. Monie, A. Aibaidula, R. Singh, I. F. Parney, Strategies, considerations, and recent advancements in the development of liquid biopsy for glioblastoma: A step towards individualized medicine in glioblastoma. *Neurosurg. Focus* **53**, E14 (2022).
14. R. H. Eibl, M. Schneemann, Liquid biopsy and glioblastoma. *Explor. Target. Antitumor Ther.* **4**, 28–41 (2023).
15. K. K. H. Yu, S. Basu, G. Baquer, R. Ahn, J. Gantchev, S. Jindal, M. S. Regan, Z. Abou-Mrad, M. C. Prabhu, M. J. Williams, A. D. D'Souza, S. W. Malinowski, K. Hopland, Y. Elhanati, S. A. Stopka, A. Stortchevoi, C. Couturier, Z. He, J. Sun, Y. Chen, A. B. Espejo, K. H. Chow, S. Yerrum, P. L. Kao, B. P. Kerrigan, L. Norberg, D. Nielsen, G. B. M. TeamLab, V. K. Puduvalli, J. Huse, R. Beroukhim, B. Y. S. Kim, S. Goswami, A. Boire, S. Frisken, M. J. Cima, M. Holdhoff, C. G. Lucas, C. Bettegowda, S. S. Levine, T. A. Bale, C. Brennan, D. A. Reardon, F. F. Lang, E. A. Chiocca, K. L. Ligon, F. M. White, P. Sharma, V. Tabar, N. Y. R. Agar, Investigative needle core biopsies support multimodal deep-data generation in glioblastoma. *Nat. Commun.* **16**, 3957 (2025).
16. A. L. Ling, I. H. Solomon, A. M. Landivar, H. Nakashima, J. K. Woods, A. Santos, N. Masud, G. Fell, X. Mo, A. S. Yilmaz, J. Grant, A. Zhang, J. D. Bernstock, E. Torio, H. Ito, J. Liu, N. Shono, M. O. Nowicki, D. Triggs, P. Halloran, R. Piranlioglu, H. Soni, B. Stopa, W. L. Bi, P. Peruzzi, E. Chen, S. W. Malinowski, M. C. Prabhu, Y. Zeng, A. Carlisle, S. J. Rodig, P. Y. Wen, E. Q. Lee, L. Nayak, U. Chukwueke, L. N. Gonzalez Castro, S. D. Dumont, T. Batchelor, K. Kittelberger, E. Tikhonova, N. Miheecheva, D. Tabakov, N. Shin, A. Gorbacheva, A. Shumskiy, F. Frenkel, E. Aguilar-Cordova, L. K. Aguilar, D. Krisky, J. Wechuck, A. Manzanera, C. Matheny, P. P. Tak, F. Barone, D. Kovarsky, I. Tirosh, M. L. Suva, K. W. Wucherpfennig, K. Ligon, D. A. Reardon, E. A. Chiocca, Clinical trial links oncolytic immunoactivation to survival in glioblastoma. *Nature* **623**, 157–166 (2023).
17. U. N. Chukwueke, P. Y. Wen, Use of the response assessment in neuro-oncology (RANO) criteria in clinical trials and clinical practice. *CNS Oncologia* **8**, CNS28 (2019).
18. M. A. Vogelbaum, D. Krivosheya, H. Borghei-Razavi, N. Sanai, M. Weller, W. Wick, R. Soffietti, D. A. Reardon, M. K. Aghi, E. Galanis, P. Y. Wen, M. van den Bent, S. Chang, Phase 0 and window of opportunity clinical trial design in neuro-oncology: A RANO review. *Neuro Oncol.* **22**, 1568–1579 (2020).
19. P. Y. Wen, M. van den Bent, G. Youssef, T. F. Cloughesy, B. M. Ellingson, M. Weller, E. Galanis, D. P. Barboriak, J. de Groot, M. R. Gilbert, R. Huang, A. B. Lassman, M. Mehta, A. M. Molinaro, M. Preusser, R. Rahman, L. K. Shankar, R. Stupp, J. E. Villanueva-Meyer, W. Wick, D. R. Macdonald, D. A. Reardon, M. A. Vogelbaum, S. M. Chang, RANO 2.0: Update to the response assessment in neuro-oncology criteria for high- and low-grade gliomas in adults. *J. Clin. Oncol.* **41**, 5187–5199 (2023).
20. J. R. Lin, M. Fallahi-Sichani, J. Y. Chen, P. K. Sorger, Cyclic immunofluorescence (CycIF), a highly multiplexed method for single-cell imaging. *Curr. Protoc. Chem. Biol.* **8**, 251–264 (2016).
21. J. R. Lin, B. Izar, S. Wang, C. Yapp, S. Mei, P. M. Shah, S. Santagata, P. K. Sorger, Highly multiplexed immunofluorescence imaging of human tissues and tumors using t-CyCIF and conventional optical microscopes. *eLife* **7**, e31657 (2018).
22. C. Neftel, J. Laffy, M. G. Filbin, T. Hara, M. E. Shore, G. J. Rahme, A. R. Richman, D. Silverbush, M. L. Shaw, C. M. Hebert, J. Dewitt, S. Gritsch, E. M. Perez, L. N. Gonzalez Castro, X. Lan, N. Druck, C. Rodman, D. Dionne, A. Kaplan, M. S. Bertalan, J. Small, K. Pelton, S. Becker, D. Bonal, Q. D. Nguyen, R. L. Servis, J. M. Fung, R. Mylvaganam, L. Mayr, J. Gojo, C. Haberler, R. Geyeregger, T. Czech, I. Slavc, B. V. Nahed, W. T. Curry, B. S. Carter, H. Wakimoto, P. K. Brastianos, T. T. Batchelor, A. Stemmer-Rachamimov, M. Martinez-Lage, M. P. Frosch, I. Stamenkovic, N. Riggi, E. Rheinbay, M. Monje, O. Rozenblatt-Rosen, D. P. Cahill, A. P. Patel, T. Hunter, I. M. Verma, K. L. Ligon, D. N. Louis, A. Regev, B. E. Bernstein, I. Tirosh, M. L. Suvà, An integrative model of cellular states, plasticity, and genetics for glioblastoma. *Cell* **178**, 835–849.e21 (2019).
23. A. Bagaev, N. Kotlov, K. Nomie, V. Svekolkin, A. Gafurov, O. Isaeva, N. Osokin, I. Kozlov, F. Frenkel, O. Gancharova, N. Almog, M. Tsiper, R. Ataullakhanov, N. Fowler, Conserved pan-cancer microenvironment subtypes predict response to immunotherapy. *Cancer Cell* **39**, 845–865.e7 (2021).
24. N. S. Butt, M. Kurdi, M. M. Fadul, S. Hakamy, B. M. J. Addas, E. Faizo, S. Alkhayyat, A. K. Bamaga, T. Alsinani, Y. Katib, F. Okal, Y. Maghrabi, A. J. Sabbagh, R. Moshref, S. Albalawi, A. Alkhotani, F. Mohammed, N. Mulla, S. Baeesa, Major Histocompatibility Class-I (MHC-I) downregulation in glioblastoma is a poor prognostic factor but not a predictive indicator for treatment failure. *Pathol. Res. Pract.* **250**, 154816 (2023).
25. L. G. Almeida, N. J. Sakabe, A. R. deOliveira, M. C. Silva, A. S. Mundstein, T. Cohen, Y.-T. Chen, R. Chua, S. Gurung, S. Gnjatic, A. A. Jungbluth, O. L. Caballero, A. Bairoch, E. Kiesler, S. L. White, A. J. Simpson, L. J. Old, A. A. Camargo, A. T. R. Vasconcelos, CTdatabase: A knowledge-base of high-throughput and curated data on cancer-testis antigens. *Nucleic Acids Res.* **37**, D816–D819 (2009).
26. F. Li, C. Liu, W. Nong, L. Lin, Y. Ge, B. Luo, S. Xiao, Q. Zhang, X. Xie, Identification of potential biomarkers in cancer testis antigens for glioblastoma. *Am. J. Transl. Res.* **15**, 799–816 (2023).
27. M. C. Neidert, D. J. Kowalewski, M. Silginer, K. Kapolou, L. Backert, L. K. Freudenmann, J. K. Peper, A. Marcu, S. S. Wang, J. S. Walz, F. Wolpert, H. G. Rammensee, R. Henschler, K. Lamszus, M. Westphal, P. Roth, L. Regli, S. Stevanovic, M. Weller, G. Eisele, The natural HLA ligandome of glioblastoma stem-like cells: Antigen discovery for T cell-based immunotherapy. *Acta Neuropathol.* **135**, 923–938 (2018).
28. C. Wang, Y. Gu, K. Zhang, K. Xie, M. Zhu, N. Dai, Y. Jiang, X. Guo, M. Liu, J. Dai, L. Wu, G. Jin, H. Ma, T. Jiang, R. Yin, Y. Xia, L. Liu, S. Wang, B. Shen, R. Huo, Q. Wang, L. Xu, L. Yang, X. Huang, H. Shen, J. Sha, Z. Hu, Systematic identification of genes with a cancer-testis expression pattern in 19 cancer types. *Nat. Commun.* **7**, 10499 (2016).
29. J. Yu, L. Wang, X. Kong, Y. Cao, M. Zhang, Z. Sun, Y. Liu, J. Wang, B. Shen, X. Bo, J. Feng, CAD v1.0: Cancer antigens database platform for cancer antigen algorithm development and information exploration. *Front. Bioeng. Biotechnol.* **10**, 819583 (2022).
30. K. Weke, S. Kote, J. Faktor, S. Al Shboul, N. Uwugiaren, P. M. Brennan, D. R. Goodlett, T. R. Hupp, I. Dapic, DIA-MS proteome analysis of formalin-fixed paraffin-embedded glioblastoma tissues. *Anal. Chim. Acta* **1204**, 339695 (2022).
31. M. J. Herpers, F. C. Ramaekers, J. Aldeweireldt, O. Moesker, J. Slooff, Co-expression of glial fibrillary acidic protein- and vimentin-type intermediate filaments in human astrocytomas. *Acta Neuropathol.* **70**, 333–339 (1986).
32. D. B. Hoelzinger, L. Mariani, J. Weis, T. Woyke, T. J. Berens, W. S. McDonough, A. Sloan, S. W. Coons, M. E. Berens, Gene expression profile of glioblastoma multiforme invasive phenotype points to new therapeutic targets. *Neoplasia* **7**, 7–16 (2005).

33. O. Skalli, U. Wilhelmsson, C. Orndahl, B. Fekete, K. Malmgren, B. Rydenhag, M. Pekny, Astrocytoma grade IV (glioblastoma multiforme) displays 3 subtypes with unique expression profiles of intermediate filament proteins. *Hum. Pathol.* **44**, 2081–2088 (2013).
34. C. Kubelt, K. Hattermann, S. Sebens, H. M. Mehdorn, J. Held-Feindt, Epithelial-to-mesenchymal transition in paired human primary and recurrent glioblastomas. *Int. J. Oncol.* **46**, 2515–2525 (2015).
35. K. Natesh, D. Bhosale, A. Desai, G. Chandrika, R. Pujari, J. Jagtap, A. Chugh, D. Ranade, P. Shastry, Oncostatin-M differentially regulates mesenchymal and proneural signature genes in gliomas via STAT3 signaling. *Neoplasia* **17**, 225–237 (2015).
36. J. Zhao, L. Zhang, X. Dong, L. Liu, L. Huo, H. Chen, High expression of vimentin is associated with progression and a poor outcome in glioblastoma. *Appl. Immunohistochem. Mol. Morphol.* **26**, 337–344 (2018).
37. A. Zottel, I. Jovčevska, N. Šamec, R. Komel, Cytoskeletal proteins as glioblastoma biomarkers and targets for therapy: A systematic review. *Crit. Rev. Oncol. Hematol.* **160**, 103283 (2021).
38. P. A. Valdes, C. J. Yu, J. Aronson, D. Ghosh, Y. Zhao, B. An, J. D. Bernstock, D. Bhere, M. M. Felicella, M. S. Viapiano, K. Shah, E. A. Chiocca, E. S. Boyden, Improved immunostaining of nanostructures and cells in human brain specimens through expansion-mediated protein decrowding. *Sci. Transl. Med.* **16**, eabo0049 (2024).
39. V. Thorsson, D. L. Gibbs, S. D. Brown, D. Wolf, D. S. Bortone, T. H. O. Yang, E. Porta-Pardo, G. F. Gao, C. L. Plaisier, J. A. Eddy, E. Ziv, A. C. Culhane, E. O. Paull, I. K. A. Sivakumar, A. J. Gentles, R. Malhotra, F. Farshidfar, A. Colaprico, J. S. Parker, L. E. Mose, N. S. Vo, J. Liu, Y. Liu, J. Rader, V. Dhankani, S. M. Reynolds, R. Bowlby, A. Califano, A. D. Cherniack, D. Anastassiou, D. Bedognetti, Y. Mokrab, A. M. Newman, A. Rao, K. Chen, A. Krasnitz, H. Hu, T. M. Malta, H. Noushmehr, C. S. Pedamallu, S. Bullman, A. I. Ojesina, A. Lamb, W. Zhou, H. Shen, T. K. Choueiri, J. N. Weinstein, J. Guinney, J. Saltz, R. A. Holt, C. S. Rabkin, Cancer Genome Atlas Research Network, A. J. Lazar, J. S. Serody, E. G. Demicco, M. L. Disis, B. G. Vincent, I. Shmulevich, The immune landscape of cancer. *Immunity* **48**, 812–830.e14 (2018).
40. V. Andreani, S. Ramamoorthy, A. Pandey, E. Lupar, S. L. Nutt, T. Lammermann, R. Grosschedl, Cochaperone Mzb1 is a key effector of Blimp1 in plasma cell differentiation and β1-integrin function. *Proc. Natl. Acad. Sci. U.S.A.* **115**, E9630–E9639 (2018).
41. M. Rosenbaum, V. Andreani, T. Kapoor, S. Herp, H. Flach, M. Duchniewicz, R. Grosschedl, MZB1 is a GRP94 cochaperone that enables proper immunoglobulin heavy chain biosynthesis upon ER stress. *Genes Dev.* **28**, 1165–1178 (2014).
42. D. J. Todd, L. J. McHeyzer-Williams, C. Kowal, A. H. Lee, B. T. Volpe, B. Diamond, M. G. McHeyzer-Williams, L. H. Glimcher, XBP1 governs late events in plasma cell differentiation and is not required for antigen-specific memory B cell development. *J. Exp. Med.* **206**, 2151–2159 (2009).
43. J. L. Halliley, C. M. Tipton, J. Liesveld, A. F. Rosenberg, J. Darce, I. V. Gregoretti, L. Popova, D. Kaminiski, C. F. Fucile, I. Albizua, S. Kyu, K. Y. Chiang, K. T. Bradley, R. Burack, M. Slifka, E. Hammarlund, H. Wu, L. Zhao, E. E. Walsh, A. R. Falsey, T. D. Randall, W. C. Cheung, I. Sanz, F. E.-H. Lee, Long-lived plasma cells are contained within the $CD19^{-}CD38^{hi}CD138^{+}$ subset in human bone marrow. *Immunity* **43**, 132–145 (2015).
44. N. Benhamouda, I. Sam, N. Epaillard, A. Gey, L. Phan, H. P. Pham, N. Gruel, A. Saldmann, J. Pineau, M. Hasan, V. Quiniou, C. Nevoret, V. Verkarre, V. Libri, S. Mella, C. Granier, C. Broudin, P. Ravel, E. De Guillebon, L. Mauge, D. Helley, B. Jabla, N. Chaput, L. Albiges, S. Katsahian, J. Adam, A. Mejean, O. Adotevi, Y. A. Vano, S. Oudard, E. Tartour, Plasma CD27, a surrogate of the intratumoral CD27-CD70 interaction, correlates with immunotherapy resistance in renal cell carcinoma. *Clin. Cancer Res.* **28**, 4983–4994 (2022).
45. J. Huggins, T. Pellegrin, R. E. Felgar, C. Wei, M. Brown, B. Zheng, E. C. Milner, S. H. Bernstein, I. Sanz, M. S. Zand, CpG DNA activation and plasma-cell differentiation of CD27- naive human B cells. *Blood* **109**, 1611–1619 (2007).
46. J. Yeong, J. C. T. Lim, B. Lee, H. Li, N. Chia, C. C. H. Ong, W. K. Lye, T. C. Putti, R. Dent, E. Lim, A. A. Thike, P. H. Tan, J. Iqbal, High densities of tumor-associated plasma cells predict improved prognosis in triple negative breast cancer. *Front. Immunol.* **9**, 1209 (2018).
47. S. Darmanis, S. A. Sloan, D. Croote, M. Mignardi, S. Chernikova, P. Samghababi, Y. Zhang, N. Neff, M. Kowarsky, C. Caneda, G. Li, S. D. Chang, I. D. Connolly, Y. Li, B. A. Barres, M. H. Gephart, S. R. Quake, Single-cell RNA-seq analysis of infiltrating neoplastic cells at the migrating front of human glioblastoma. *Cell Rep.* **21**, 1399–1410 (2017).
48. S. Muller, G. Kohanbash, S. J. Liu, B. Alvarado, D. Carrera, A. Bhaduri, P. B. Watchmaker, G. Yagnik, E. Di Lullo, M. Malatesta, N. M. Amankulor, A. R. Kriegstein, D. A. Lim, M. Aghi, H. Okada, A. Diaz, Single-cell profiling of human gliomas reveals macrophage ontogeny as a basis for regional differences in macrophage activation in the tumor microenvironment. *Genome Biol.* **18**, 234 (2017).
49. S. Goswami, T. Walle, A. E. Cornish, S. Basu, S. Anandhan, I. Fernandez, L. Vence, J. Blando, H. Zhao, S. S. Yadav, M. Ott, L. Y. Kong, A. B. Heimberger, J. de Groot, B. Sepesi, M. Overman, S. Kopetz, J. P. Allison, D. Pe'er, P. Sharma, Immune profiling of human tumors identifies CD73 as a combinatorial target in glioblastoma. *Nat. Med.* **26**, 39–46 (2020).
50. N. Abdelfattah, P. Kumar, C. Wang, J. S. Leu, W. F. Flynn, R. Gao, D. S. Baskin, K. Pichumani, O. B. Ijare, S. L. Wood, S. Z. Powell, D. L. Haviland, B. C. Parker Kerrigan, F. F. Lang, S. S. Prabhu, K. M. Huntoon, W. Jiang, B. Y. S. Kim, J. George, K. Yun, Single-cell analysis of human glioma and immune cells identifies S100A4 as an immunotherapy target. *Nat. Commun.* **13**, 767 (2022).
51. A. B. Afeyan, C. J. Wu, G. Oliveira, Rapid parallel reconstruction and specificity screening of hundreds of T cell receptors. *Nat. Protoc.* **20**, 539–586 (2025).
52. A. M. Luoma, S. Suo, Y. Wang, L. Gunasti, C. B. M. Porter, N. Nabilsi, J. Tadros, A. P. Ferretti, S. Liao, C. Gurer, Y. H. Chen, S. Criscitiello, C. A. Ricker, D. Dionne, O. Rozenblatt-Rosen, R. Uppaluri, R. I. Haddad, O. Ashenberg, A. Regev, E. M. Van Allen, G. MacBeath, J. D. Schoenfeld, K. W. Wucherpfennig, Tissue-resident memory and circulating T cells are early responders to pre-surgical cancer immunotherapy. *Cell* **185**, 2918–2935.e29 (2022).
53. L. K. Mackay, M. Minnich, N. A. M. Kragten, Y. Liao, B. Nota, C. Seillet, A. Zaid, K. Man, S. Preston, D. Freestone, A. Braun, E. Wynne-Jones, F. M. Behr, R. Stark, D. G. Pellicci, D. I. Godfrey, G. T. Belz, M. Pellegrini, T. Gebhardt, M. Busslinger, W. Shi, F. R. Carbone, R. A. W. van Lier, A. Kallies, K. P. J. M. van Gisbergen, Hobit and Blimp1 instruct a universal transcriptional program of tissue residency in lymphocytes. *Science* **352**, 459–463 (2016).
54. G. Oliveira, A. M. Egloff, A. B. Afeyan, J. O. Wolff, Z. Zeng, R. D. Chernock, L. Zhou, C. Messier, P. Lizotte, K. L. Pfaff, K. Stromhaug, L. Penter, R. I. Haddad, G. J. Hanna, J. D. Schoenfeld, L. A. Goguen, D. J. Annino, V. Jo, P. Oppelt, P. Pipkorn, R. Jackson, S. V. Puram, R. C. Paniello, J. T. Rich, J. Webb, J. P. Zevallos, M. Mansour, J. Fu, G. P. Dunn, S. J. Rodig, J. Ley, L. G. T. Morris, L. Dunn, C. P. Paweletz, D. Kallogjeri, J. F. Piccirillo, D. R. Adkins, C. J. Wu, R. Uppaluri, Preexisting tumor-resident T cells with cytotoxic potential associate with response to neoadjuvant anti-PD-1 in head and neck cancer. *Sci. Immunol.* **8**, eadf4968 (2023).
55. L. Parga-Vidal, F. M. Behr, N. A. M. Kragten, B. Nota, T. H. Wesselink, I. Kavazović, L. E. Covill, M. B. P. Schuller, Y. T. Bryceson, F. M. Wensveen, R. A. W. van Lier, T. J. P. van Dam, R. Stark, K. P. J. M. van Gisbergen, Hobit identifies tissue-resident memory T cell precursors that are regulated by Eomes. *Sci. Immunol.* **6**, eabg3533 (2021).
56. E. M. Parry, C. K. Lemvigh, S. Deng, N. Dangle, N. Ruthen, B. A. Knisbacher, J. Broseus, S. Hergalant, R. Guieze, S. Li, W. Zhang, C. Johnson, J. M. Long, S. Yin, L. Werner, A. Anandappa, N. Purroy, S. Gohil, G. Oliveira, P. Bachireddy, S. A. Shukla, T. Huang, J. D. Khoury, B. Thakral, M. Dickinson, C. Tam, K. J. Livak, G. Getz, D. Neuberg, P. Feugier, P. Kharchenko, W. Wierda, L. R. Olsen, N. Jain, C. J. Wu, ZNF683 marks a $CD8^{+}$ T cell population associated with anti-tumor immunity following anti-PD-1 therapy for Richter syndrome. *Cancer Cell* **41**, 1803–1816.e8 (2023).
57. P. Y. Wen, D. R. Macdonald, D. A. Reardon, T. F. Cloughesy, A. G. Sorensen, E. Galanis, J. Degroot, W. Wick, M. R. Gilbert, A. B. Lassman, C. Tsien, T. Mikkelsen, E. T. Wong, M. C. Chamberlain, R. Stupp, K. R. Lamborn, M. A. Vogelbaum, M. J. van den Bent, S. M. Chang, Updated response assessment criteria for high-grade gliomas: Response assessment in neuro-oncology working group. *J. Clin. Oncol.* **28**, 1963–1972 (2010).
58. M. F. Gjerstorff, M. H. Andersen, H. J. Ditzel, Oncogenic cancer/testis antigens: Prime candidates for immunotherapy. *Oncotarget* **6**, 15772–15787 (2015).
59. M. Freitas, S. Malheiros, J. N. Stávale, T. P. Biassi, F. T. Zamunér, M. de Souza Begnami, F. A. Soares, A. L. Vettore, Expression of cancer/testis antigens is correlated with improved survival in glioblastoma. *Oncotarget* **4**, 636–646 (2013).
60. S. Ghafouri-Fard, M. H. Modarressi, Expression of cancer-testis genes in brain tumors: Implications for cancer immunotherapy. *Immunotherapy* **4**, 59–75 (2012).
61. E. A. Chiocca, H. Nakashima, K. Kasai, S. A. Fernandez, M. Oglesbee, Preclinical toxicology of rQNestin34.5v.2: An oncolytic herpes virus with transcriptional regulation of the ICP34.5 neurovirulence gene. *Mol. Ther. Methods Clin. Dev.* **17**, 871–893 (2020).
62. Y. Yuan, J. Wu, M. R. Gilbert, BOIN: A novel Bayesian design platform to accelerate early phase brain tumor clinical trials. *Neurooncol. Pract.* **8**, 627–638 (2021).
63. K. Krug, P. Mertins, B. Zhang, P. Hornbeck, R. Raju, R. Ahmad, M. Szucs, F. Mundt, D. Forestier, J. Jane-Valbuena, H. Keshishian, M. A. Gillette, P. Tamayo, J. P. Mesirov, J. D. Jaffe, S. A. Carr, D. R. Mani, A curated resource for phosphosite-specific signature analysis. *Mol. Cell. Proteomics* **18**, 576–593 (2019).
64. D. A. Barbie, P. Tamayo, J. S. Boehm, S. Y. Kim, S. E. Moody, I. F. Dunn, A. C. Schinzel, P. Sandy, E. Meylan, C. Scholl, S. Frohling, E. M. Chan, M. L. Sos, K. Michel, C. Mermel, S. J. Silver, B. A. Weir, J. H. Reiling, Q. Sheng, P. B. Gupta, R. C. Wadlow, H. Le, S. Hoersch, B. S. Wittner, S. Ramaswamy, D. M. Livingston, D. M. Sabatini, M. Meyerson, R. K. Thomas, E. S. Lander, J. P. Mesirov, D. E. Root, D. G. Gilliland, T. Jacks, W. C. Hahn, Systematic RNA interference reveals that oncogenic *KRAS*-driven cancers require TBK1. *Nature* **462**, 108–112 (2009).
65. M. E. Abazeed, D. J. Adams, K. E. Hurov, P. Tamayo, C. J. Creighton, D. Sonkin, A. O. Giacomelli, C. Du, D. F. Fries, K. K. Wong, J. P. Mesirov, J. S. Loeffler, S. L. Schreiber, P. S. Hammerman, M. Meyerson, Integrative radiogenomic profiling of squamous cell lung cancer. *Cancer Res.* **73**, 6289–6298 (2013).
66. H. Kambara, H. Okano, E. A. Chiocca, Y. Saeki, An oncolytic HSV-1 mutant expressing ICP34.5 under control of a nestin promoter increases survival of animals even when symptomatic from a brain tumor. *Cancer Res.* **65**, 2832–2839 (2005).
67. M. Jenkinson, S. Smith, A global optimisation method for robust affine registration of brain images. *Med. Image Anal.* **5**, 143–156 (2001).

68. M. Jenkinson, P. Bannister, M. Brady, S. Smith, Improved optimization for the robust and accurate linear registration and motion correction of brain images. *Neuroimage* **17**, 825–841 (2002).
69. F. Isensee, M. Schell, I. Pflueger, G. Brugnara, D. Bonekamp, U. Neuberger, A. Wick, H. P. Schlemmer, S. Heiland, W. Wick, M. Bendszus, K. H. Maier-Hein, P. Kickingereder, Automated brain extraction of multisequence MRI using artificial neural networks. *Hum. Brain Mapp.* **40**, 4952–4964 (2019).
70. A. Fedorov, R. Beichel, J. Kalpathy-Cramer, J. Finet, J. C. Fillion-Robin, S. Pujol, C. Bauer, D. Jennings, F. Fennessy, M. Sonka, J. Buatti, S. Aylward, J. V. Miller, S. Pieper, R. Kikinis, 3D Slicer as an image computing platform for the quantitative imaging network. *Magn. Reson. Imaging* **30**, 1323–1341 (2012).
71. K. K. H. Yu, S. Basu, G. Baquer, R. Ahn, J. Gantchev, S. Jindal, M. S. Regan, Z. Abou-Mrad, M. C. Prabhu, M. J. Williams, A. D. D'Souza, S. W. Malinowski, K. Hopland, Y. Elhanati, S. A. Stopka, A. Stortchevoi, Z. He, J. Sun, Y. Chen, A. B. Espejo, K. H. Chow, S. Yerrum, P. L. Kao, B. P. Kerrigan, L. Norberg, D. Nielsen, G. B. M. TeamLab, V. K. Puduvalli, J. Huse, R. Beroukhim, Y. S. B. Kim, S. Goswami, A. Boire, S. Frisken, M. J. Cima, M. Holdhoff, C. G. Lucas, C. Bettegowda, S. S. Levine, T. A. Bale, C. Brennan, D. A. Reardon, F. F. Lang, E. Antonio Chiocca, K. L. Ligon, F. M. White, P. Sharma, V. Tabar, N. Y. R. Agar, Investigative needle core biopsies for multi-omics in glioblastoma. medRxiv 23300541 [Preprint] (2023); https://doi.org/10.1101/2023.12.29.23300541.
72. G. Ayoub, D. Elharouni, C. Bossi, C. Möller, S. Malinowski, J. Japo, A. J. Vaidya, A. Zhang, M. Shaban, A. Santos, D. Williamson, D. Meredith, F. Mahmood, K. Ligon, PATH-50. AI-powered automated tissue segmentation improves outcome stratification in glioblastoma. *Neuro Oncol.* **26**, viii190 (2024).
73. S. Coy, S. Wang, S. A. Stopka, J. R. Lin, C. Yapp, C. C. Ritch, L. Salhi, G. J. Baker, R. Rashid, G. Baquer, M. Regan, P. Khadka, K. A. Cole, J. Hwang, P. Y. Wen, P. Bandopadhayay, M. Santi, T. De Raedt, K. L. Ligon, N. Y. R. Agar, P. K. Sorger, M. Touat, S. Santagata, Single cell spatial analysis reveals the topology of immunomodulatory purinergic signaling in glioblastoma. *Nat. Commun.* **13**, 4814 (2022).
74. D. Schapiro, A. Sokolov, C. Yapp, Y. A. Chen, J. L. Muhlich, J. Hess, A. L. Creason, A. J. Nirmal, G. J. Baker, M. K. Nariya, J. R. Lin, Z. Maliga, C. A. Jacobson, M. W. Hodgman, J. Ruokonen, S. L. Farhi, D. Abbondanza, E. T. McKinley, D. Persson, C. Betts, S. Sivagnanam, A. Regev, J. Goecks, R. J. Coffey, L. M. Coussens, S. Santagata, P. K. Sorger, MCMICRO: A scalable, modular image-processing pipeline for multiplexed tissue imaging. *Nat. Methods* **19**, 311–315 (2022).
75. J. L. Muhlich, Y. A. Chen, C. Yapp, D. Russell, S. Santagata, P. K. Sorger, Stitching and registering highly multiplexed whole-slide images of tissues and tumors using ASHLAR. *Bioinformatics* **38**, 4613–4621 (2022).
76. C. Soneson, M. I. Love, M. D. Robinson, Differential analyses for RNA-seq: Transcript-level estimates improve gene-level inferences. *F1000Res* **4**, 1521 (2015).
77. M. Reich, T. Liefeld, J. Gould, J. Lerner, P. Tamayo, J. P. Mesirov, GenePattern 2.0. *Nat. Genet.* **38**, 500–501 (2006).
78. Y. Hao, S. Hao, E. Andersen-Nissen, W. M. Mauck III, S. Zheng, A. Butler, M. J. Lee, A. J. Wilk, C. Darby, M. Zager, P. Hoffman, M. Stoeckius, E. Papalexi, E. P. Mimitou, J. Jain, A. Srivastava, T. Stuart, L. M. Fleming, B. Yeung, A. J. Rogers, J. M. McElrath, C. A. Blish, R. Gottardo, P. Smibert, R. Satija, Integrated analysis of multimodal single-cell data. *Cell* **184**, 3573–3587.e29 (2021).
79. I. Korsunsky, N. Millard, J. Fan, K. Slowikowski, F. Zhang, K. Wei, Y. Baglaenko, M. Brenner, P. R. Loh, S. Raychaudhuri, Fast, sensitive and accurate integration of single-cell data with Harmony. *Nat. Methods* **16**, 1289–1296 (2019).
80. J. B. Iorgulescu, N. Ruthen, R. Ahn, E. Panagioti, P. C. Gokhale, M. Neagu, M. C. Speranza, B. K. Eschle, K. M. Soroko, R. Piranlioglu, M. Datta, S. Krishnan, K. B. Yates, G. J. Baker, R. K. Jain, M. L. Suva, D. Neuberg, F. M. White, E. A. Chiocca, G. J. Freeman, A. H. Sharpe, C. J. Wu, D. A. Reardon, Antigen presentation deficiency, mesenchymal differentiation, and resistance to immunotherapy in the murine syngeneic CT2A tumor model. *Front. Immunol.* **14**, 1297932 (2023).
81. L. Kall, J. D. Canterbury, J. Weston, W. S. Noble, M. J. MacCoss, Semi-supervised learning for peptide identification from shotgun proteomics datasets. *Nat. Methods* **4**, 923–925 (2007).
82. J. L. Johnson, T. M. Yaron, E. M. Huntsman, A. Kerelsky, J. Song, A. Regev, T. Y. Lin, K. Liberatore, D. M. Cizin, B. M. Cohen, N. Vasan, Y. Ma, K. Krismer, J. T. Robles, B. van de Kooij, A. E. van Vlimmeren, N. Andree-Busch, N. F. Kaufer, M. V. Dorovkov, A. G. Ryazanov, Y. Takagi, E. R. Kastenhuber, M. D. Goncalves, B. D. Hopkins, O. Elemento, D. J. Taatjes, A. Maucuer, A. Yamashita, A. Degterev, M. Uduman, J. Lu, S. D. Landry, B. Zhang, I. Cossentino, R. Linding, J. Blenis, P. V. Hornbeck, B. E. Turk, M. B. Yaffe, L. C. Cantley, An atlas of substrate specificities for the human serine/threonine kinome. *Nature* **613**, 759–766 (2023).
83. A. Liberzon, C. Birger, H. Thorvaldsdottir, M. Ghandi, J. P. Mesirov, P. Tamayo, The Molecular Signatures Database (MSigDB) hallmark gene set collection. *Cell Syst.* **1**, 417–425 (2015).
84. P. Langfelder, S. Horvath, WGCNA: An R package for weighted correlation network analysis. *BMC Bioinformatics* **9**, 559 (2008).
85. M. V. Kuleshov, M. R. Jones, A. D. Rouillard, N. F. Fernandez, Q. Duan, Z. Wang, S. Koplev, S. L. Jenkins, K. M. Jagodnik, A. Lachmann, M. G. McDermott, C. D. Monteiro, G. W. Gundersen, A. Ma'ayan, Enrichr: A comprehensive gene set enrichment analysis web server 2016 update. *Nucleic Acids Res.* **44**, W90–W97 (2016).
86. L. E. Stopfer, J. M. Mesfin, B. A. Joughin, D. A. Lauffenburger, F. M. White, Multiplexed relative and absolute quantitative immunopeptidomics reveals MHC I repertoire alterations induced by CDK4/6 inhibition. *Nat. Commun.* **11**, 2760 (2020).

Acknowledgments: We are deeply indebted to the participants and their families for support, courage, and enthusiasm. We gratefully acknowledge all of the patients and families who have participated in the trial so far and all of the dedicated members of the GBM TeamLab across the Break Through Cancer network. **Funding:** This work was supported by Break Through Cancer (Cambridge, MA), the National Cancer Institute P01 CA163205 (to EAC), National Cancer Institute P01 CA236749 (to E.A.C. and D.A.R.), and the National Institutes of Health R01NS110942 (to E.A.C.). Candel Therapeutics Inc. provided in-kind support. G.O. was supported by the Claudia Adams Barr Program for Innovative Cancer Research. **Author contributions:** The Accelerating GBM Therapies TeamLab members (main and supplementary authors) were responsible for the overall concepts, methods, hypotheses, funding proposal writing, and methodologies shown in this manuscript through multiple meetings and discussions from the early months of 2020 until the present. F.F.L., V.K.P., V.T., M.H., C.B., M.C., P.P.T., P.S., F.M.W., K.L.L., N.Y.R.A., D.A.R., and E.A.C. acquired the funding for this study. A.L.L., D.A.R., S.B., P.S., A.D., R.A., F.M.W., G.O., and E.A.C. wrote the original draft of the manuscript. A.L.L., D.A.R., N.M., G.R.V., J.G., M.S.R., N.Y.R.A., Z.A.-M., A.S., G.A., C.P.C., D.E., M.C.P., J.V., I.H.S., K.L.L., P.P.T., Y.Y., C.A.W., A.D., R.A., F.M.W., S.B., H.C., Z.H., P.S., W.J., F.L.L., V.K.P., V.T., K.K.H.Y., C.W.B., A.B., M.H., C.B., C.H.L., G.O., and E.A.C. reviewed and edited the manuscript. A.L.L., C.P.C., K.K.H.Y., C.A.W., and E.A.C. developed the multimodal integration. J.G., M.C.P., N.M., G.R.V., M.S.R., K.K.H.Y., F.F.L., V.K.P., V.T., C.W.B., A.B., M.H., C.B., M.C., H.E.S., Y.Y., P.P.T., P.S., F.M.W., K.L.L., N.Y.R.A., D.A.R., and E.A.C. contributed to Fig. 1. A.L.L., J.G., G.B., Z.A.-M., A.S., G.A., D.E., J.V., K.L.L., N.Y.R.A., and E.A.C. contributed to Fig. 2 and figs. S1 to S3. J.G., M.S.R., G.B., and N.Y.R.A. contributed to fig. S4. S.B., Z.A.-M., C.P.C., K.K.H.Y., V.T., C.B., C.A.W., and P.S. contributed to fig. S5. R.A., A.D., and F.M.W. contributed to Fig. 3 and figs. S6 to S11. S.B., H.C., Z.H., and P.S. contributed to Fig. 4 and figs. S12 and S13. H.E.S., G.O., A.L.L., and E.A.C. contributed to Fig. 5 and figs. S14 and S15. A.L.L. and E.A.C. designed fig. S16. M.C.P., N.M., A.B., O.N., G.R.V., D.A.R., and E.A.C. generated tables S1, S2, S4, and S5. J.G., M.S.R., G.B., and N.Y.R.A. generated table S3. A.L.L. and E.A.C. generated movie files S1 and S2 and data files S1 and S2. **Competing interests:** A.D. is a venture fellow with ARTIS Ventures. M.S.R. is a consultant for Bondz LLC. C.H.L. is a consultant for Servier. V.K.P. reports serving on the advisory boards or as a consultant for Orbus Therapeutics, Servier, Novocure, Insightec, Telix Pharmaceuticals, Tango Therapeutics, Guidepoint Inc., Bayer, Boehringer Ingelheim, MD HealthGroup, and Bexion. V.K.P. has received research funding from Bexion, Kazia Therapeutics, Servier, Radiomedix, Karyopharm Therapeutics, Samus Therapeutics, Insightec, Merck, Philogen, Equity, and Gilead. V.K.P. has uncompensated relationships with Remedy Plan Therapeutics and Aqualung Therapeutics. V.T. is a scientific advisor and receives research support from BlueRock Therapeutics, is a scientific advisor to Robeaute and Ajax Healthcare, is a member of the Scientific Advisory Board of St Jude's Children's Research Hospital, and is an unpaid trustee on the Board of Trustees of the American University of Beirut. A.B. holds an unpaid position on the scientific advisory board for Evren Technologies and is an inventor on the following patents: 62/258,044, 10/413,522, and 63/052,139; the US provisional patent application nos. 63/449,817 and 63/449,823; and the international patent application no. PCT/US24/18343 filed by MSKCC. M.H. reports serving on the advisory boards or as a consultant for Servier, AnHeart, Novartis, and Bayer. M.H. is on the data safety monitoring board of Advarra and Parexel. M.H. is on the steering committee for a clinical trial for Novartis and receives honoraria from Novartis. C.W.B. is a consultant for Depuy Synthes, Bionaut Labs, Haystack Oncology, and Privo Technologies. C.B. is a cofounder of Belay Diagnostics and OrisDx. M.C. is a consultant to Dare Bioscience, a consultant to Johnson and Johnson, a director at GelMEDIX Inc, and a director and founder at Stratagen Bio. Y.Y. is a statistical consultant for AbbVie, Aktis Oncology, Affinixttx, Amgen, Astellas, Avance, Bexion, BioNTech, Blueprint, Boehringer Ingelheim, Boren Hospital, BrainChildBio, Bristol Myers Squibb, Century Therapeutics, Cogent, CoRegen, GenAssist, Genesis Therapeutic, GT Medical, Kyowa Kirin, Merck, NGM Bio, Point Biopharma, NextCure, Repare, Sangamo, Score Innovation, Schrodinger, Servier, Umajo, and Vertex. P.P.T. is president, CEO, and shareholder of Candel Therapeutics; chair of the board of Citryll; board director of Sitryx; board director of Levicept; consultant to NovoNordisk; consultant to SecondWave Systems; and consultant to Byondis [patent application no. 63/703, 120 filed on 10/03/2024 Candel docket CAND-019USPR. Title: Compositions and methods for treating melanoma using an oncolytic virus; status: pending US provisional application (expected exp, if nationalized and issued, 2045)]. P.S. is a scientific advisory committee member of Achelois, Affini-T, Akoya Biosciences, Apricity, Asher Bio, BioAtla LLC, Candel Therapeutics, Catalio, C-Reveal Therapeutics, Dragonfly Therapeutics, Earli Inc, Enable Medicine, Glympse, Henlius/Hengenix, Hummingbird, ImaginAb, InterVenn Biosciences, LAVA Therapeutics, Lytix Biopharma, Marker Therapeutics, Matrisome, NTx, Oncolytics, Osteologic, PBM Capital, Phenomic AI, Polaris Pharma, Soley Therpeutics, Spotlight, Trained Therapeutix Discovery, Two Bear Capital, Vironexis, and Xilis Inc.; private investment in Adaptive Biotechnologies, Time Bioventures, JSL Health, BioNTech, and Sporos. F.M.W. is a consultant for Travera and Servier and holds equity in Travera. N.Y.R.A. is a KOL for Bruker; consultant and on the scientific advisory board for National

Brain Tumor Society; received research support from Thermo, EMD Serono, and iTeos Therapeutics; and is a scientific founder of BondZ LLC. D.A.R. is a consultant or advisory board member since 2021 for AnHeart Pharmaceuticals; Aptitude Health; BlueRock Therapeutics LP; CeCaVaGmbH & Co.KG; Chimeric Therapeutics; Elsevier; F. Hoffman La-Roche; Genenta Science; Inovio; Insightec; Janssen; Jupiter Life Sciences Consulting, LLC; Kintara; Kiyatec; Johnson & Johnson, Pharma; Lumanity; Menari Stemline; Miltenyi Biomedicine GmbH; Neuvogen; Novocure; Paradigm Medical Communications; Putnam Inizii Associates, LLC; Sumitono Dainippon Pharma Oncology; Servier; Triangle Insights Group; Vivacitas Oncology, Inc.; and WebMD research support and for (paid to DFCI) Agenus; Ashvattha Therapeutics; Boehringer Ingelheim; Bristol-Myers Squibb; Corbus Pharma; EMD Serono; Enterome; Invios; Medicenna Therapeutics; Mogling Gio; NeoTx Ltd; Numiera Therapeutics; Sapience Therapeutics; SphereBio; and Vaccinex. G.O. is an inventor on patent "Generation of anti-tumor T-cells" (US20240091259A1). E.A.C. is currently an advisor to Bionaut Labs, Seneca Therapeutics, and Theriva; has equity options in Bionaut Laboratories, Seneca Therapeutics, Ternalys Therapeutics, and RelgnIte Therapeutics; and is cofounder and on the board of directors of Ternalys Therapeutics. He also provides or has provided (in last 2 years) unpaid scientific and clinical advice to Amacathera, Alpheus Medical, Bio TTT, Brave Bio, Calidi Biotherapeutics, Candel Therapeutics, Carthera Sonocloud, Diakonos, Genenta, Iconovir, Incephalo Therapeutics, Insightec Inc., Lumicell, Ovie Therapeutics, Rocket Science, RZnomics, and Targtex. He is a named inventor on patents related to oncolytic HSV1, including patents owned by BWH on CAN-3110 and other oHSV technologies that are now licensed to Candel Therapeutics Inc. (patent no. US10,806,761 B2, date: 20 October 2020; patent no. 6,897,057, date 24 May 2005; patent no. 7,214,515 4 January 2002) who provides milestone and royalty payments to BWH.

Data and materials availability: All data are available in the main text, the Supplementary Materials, or the following repositories. The agent, CAN-3110, used in this trial is proprietary and has been exclusively licensed by Mass General Brigham to Candel Therapeutics Inc., and it is not available. A preclinical strain (rQNestin34.5v.1) is available through an material transfer aggreement with E.A.C. Data generated in this study have been deposited in appropriate repositories for each data type. MRI scans, H&E slides, and CyCIF slides have been deposited in Figshare (https://figshare.com/; 10.6084/m9.figshare.28950887, 10.6084/m9.figshare.29822162, and 10.6084/m9.figshare.29332715). Proteomic, phosphoproteomic, and immunopeptidomic data have been deposited in PRIDE (www.ebi.ac.uk/pride/; PXD063408, PXD063976, and PXD063451). Bulk RNA-seq, scRNA-seq, and scTCR-seq data have been deposited in dbGaP (https://dbgap.ncbi.nlm.nih.gov; phs004189) and are available at https://www.ncbi.nlm.nih.gov/projects/gap/cgi-bin/study.cgi?study_id=phs004189. Custom code generated during these analyses has been deposited in Zenodo (https://zenodo.org/: MRI code: 10.5281/zenodo.15490797; TCR analysis: 10.5281/zenodo.15490784; ssGSEA: 10.5281/zenodo.15425009; InferCNV: 10.5281/zenodo.15231121; figure generation: 10.5281/zenodo.16780795).

In addition to the authors, the following Accelerating GBM Therapies TeamLab members have contributed to conceptualization of the study, development of the methodology, clinical trial investigation, and conducting of the analysis:

Jennifer Wiley[22], Kathryn Partridge[22], Rameen Beroukhim[22], Amanda Spearman[22], Ugonma N. Chukwueke[22], Patrick Y. Wen[22], Austin L.H. Chiocca[2], Sarah Frisken[1], Brian J. Coyne[1], Daniel Triggs[1], Kimberly L Vasquez[1], Michal O. Nowicki[1], Himanshu Soni[1], Raziye Piranlioglu[1], Marco Mineo[1], Ana Montalvo Landivar[1], Sylwia A. Stopka[2], Md Amin Hossain[2], Seth W. Malinowski[3,4], Sonam Bhatia[4,23], Thomas Quinn[4,23], Marla J. Polk[21], Alexsandra B. Espejo[5], Jingjing Sun[5], Yulong Chen[5], Sonali Jindal[5], Jason T Huse[24], Lisa Norberg[24], Sangeeta Goswami[5,25], Betty Y. Kim[13], Kadir C. Akdemir[13], Brittany Parker Kerrigan[13], Douglas Nielsen[13], Jian Hu[26], Pratibha Sharma[14], Chetna Wathoo[14], Gregory Buchold[14], Jiyong Liang[14], Stuart Levine[6], Qun Cao[6], Alexei Stortchevoi[6], Shahiba Ogilvie[7], Alexandra Giantini Larsen[7], Kelsey Hopland[7], Yuval Elhanati[7], Rachel Estrera[15], Isaiah Osei-Gyening[15], Tejus A. Bale[27], Christopher Douville[17], Jordina Rincon Torroella[17], Vasilena Gocheva[28], Francesca Barone[19], Jennifer Moliterno[29].
[23]Center for Patient Derived Models, Dana-Farber Cancer Institute, Boston, MA 02115, USA. [24]Department of Pathology, University of Texas MD Anderson Cancer Hospital, Houston, TX 77030, USA. [25]Department of Genitourinary Oncology, University of Texas MD Anderson Cancer Hospital, Houston, TX 77030, USA. [26]Department of Cancer Biology, University of Texas MD Anderson Cancer Hospital, Houston, TX 77030, USA. [27]Department of Pathology, Memorial Sloan Kettering Cancer Center, New York, NY 10065, USA. [28]Lustgarten Dedicated Laboratory, Dana-Farber Cancer Institute and Harvard Medical School, Boston, MA 02115, USA. [29]Department of Neurosurgery, Yale New Haven Medical Center, New Haven, CT 06510, USA.

Submitted 12 December 2024
Accepted 10 July 2025
Published 8 October 2025
10.1126/scitranslmed.adv2881